Running head: Brain-Environment Alignment

Brain-Environment Alignment during Movie Watching Predicts Cognitive-Affective Function in Adulthood

Raluca Petrican, Kim S. Graham and Andrew D. Lawrence

Cardiff University Brain Research Imaging Centre (CUBRIC), School of Psychology, Cardiff University, Maindy Road, Cardiff, CF24 4HQ, United Kingdom. Corresponding author: petricanr@cardiff.ac.uk (R.P.)

Conflict of interest. The authors declare no competing interests.

Acknowledgments. KSG and ADL were funded by grants from the Medical Research Council (MR/N01233X/1) and a Wellcome Trust Strategic Award (104943/Z/14/Z). Data were provided by the Cambridge Centre for Ageing and Neuroscience (Principal Investigator: Lorraine K. Tyler; funders: the Biotechnology and Biological Sciences Research Council, the Medical Research Council Cognition & Brain Sciences Unit and the European Union Horizon 2020 LifeBrain project) and the Human Connectome Project, WU-Minn Consortium (Principal Investigators: David Van Essen and Kamil Ugurbil; 1U54MH091657; funders: the 16 NIH Institutes and Centers that support the NIH Blueprint for Neuroscience Research and the McDonnell Center for Systems Neuroscience at Washington University).

Abstract

The brain's functional architecture changes considerably across multiple timescales. While the role of variations over long timescales (e.g., years) is widely documented, the functional relevance of microtemporal (i.e., second-level) fluctuations is still debated. Using fMRI data collected during movie watching from two independent samples, we demonstrate that the adaptiveness of variability in functional brain architecture fluctuates across the adult lifespan (18-88 years) due to age-related differences in the associated profiles of network communication. Greater coupling between changes in brain architecture and concrete environmental features is stronger at younger ages and linked to poorer cognitive-affective outcomes. Whole-brain communication pathways anchored in regions key to episodic and semantic context creation contribute to greater brain reconfiguration in response to abstract contextual changes and stronger coupling between changes in brain architecture and concrete environmental features. Our results provide new insights into age-related differences in brain-environment alignment and their relevance to cognitive adaptability and psychopathology.

Keywords: Event Cognition, Functional Networks, Dynamic Connectivity, Fluid Intelligence, Ageing, Anxiety

Brain-Environment Alignment during Movie Watching Predicts Cognitive-Affective Function in Adulthood

The human brain demonstrates significant fluctuations in functional connectivity across multiple spatial (i.e., voxels to regions) and temporal (i.e., seconds to years) scales (Poldrack & Shine, 2018). While the role of connectivity changes across long timescales (e.g., years) is widely documented, the functional relevance of micro-temporal (i.e., second-level) fluctuations is still debated, with some studies underscoring their role in maturation and learning, whereas others point to their association with accelerated cognitive aging in later life (Bassett et al., 2011, 2013; Chan et al., 2014; Gonzalez-Castillo & Bandettini, 2018; Hutchison & Morton, 2015; Mujica-Parodi et al., 2020).

To reconcile these findings, here, we probe the functional relevance of dynamic brain reconfiguration in response to naturalistic, dynamic stimuli (Sonkusare, Breakspear, & Guo, 2019; Sporns, 2013). We thus capitalise on evidence that the human mind readily breaks down the continuous influx of environmental information into meaningful units, which it uses to predict and encode ongoing experiences (Baldwin & Kosie, 2020; Kurby & Zacks, 2008). Such segmentation processes unfold at multiple timescales and give rise to a nested event hierarchy, which spans relatively frequent and readily processed low-level featural fluctuations (e.g., object presence/absence) to more sporadic and abstract, slower processed, high-level changes to the "working event model" underlying an ongoing experience (Baldassano et al., 2018; Hasson, Chen, & Honey, 2015; Zacks, 2020).

To probe the neural dynamics underlying real-life information processing, we used fMRI data collected during naturalistic movie watching paradigms, because they provide an ecologically valid framework for investigating individual and ageing-related differences in event

cognition and associated patterns of functional brain reconfiguration (Bottenhorn et al., 2019; Demirtas et al., 2019; Geerligs, Cam-Can, & Campbell, 2018; Gilson et al., 2018; Simony et al., 2016). To index the adaptiveness of functional brain reconfiguration during movie watching, we used a measure of fluid intelligence, a cognitive capacity reliant on mental segmentation proficiency, which underpins updating of event representations and is associated with greater flexibility in functional brain architecture (Barbey, 2018; Colzato, van Wouwe, Lavender, & Hommel, 2006; Duncan, Assem, & Shashidhara, 2020; Duncan, Chylinskia, Mitchell, & Bhandaric, 2017). Depression and anxiety scales gauged complementary affectively-driven biases in attention (i.e., towards abstract, schematic vs. concrete, perceptually rich information), which reportedly impact event segmentation processes (Belzung, Wilner, & Philippot, 2015; Brewin, Gregory, Lipton, & Burgess, 2010; Hermans, Henckens, Joels, & Fernandez, 2014; Petrican, Saverino, Rosenbaum, & Grady, 2015; Sherrill, Kurby, Lilly, & Magliano, 2019; Sylverster et al., 2012).

To characterise the underpinnings of functional brain reconfiguration, we draw on evidence that the human brain is organised into dissociable anatomical networks, which provide a blueprint for the brain's functional architecture (Fox & Raichle, 2007; Mesulam, 1998). Functional brain reconfiguration across multiple timescales (i.e., seconds to weeks) underlies learning and adjustment to unpredictable surroundings, while overall stability in patterns of large-scale functional network integration/separation predicts superior cognitive functioning (Alderson et al., 2020; Finc et al., 2020; Hilger, Fukushima, Sporns, & Fiebach, 2019; Kao et al., 2020). Based on this literature, we pursued several lines of inquiry regarding the relationship between global profiles of functional network interaction and dynamic brain reconfiguration during naturalistic event cognition.

There is compelling evidence that ageing impacts some of the mental processes and brain activity patterns underlying event segmentation, partly because it leads to increased reliance on conceptual, rather than perceptual, information (Kurby & Zacks, 2011, 2018; Radvansky & Dijkstra, 2007; Reagh, Delarazan, Garber, & Ranganath, 2020; Spreng & Turner, 2015). Capitalising on this, we examined whether dynamic neural reconfiguration during movie watching is linked to distinguishable profiles of functional network communication across the adult lifespan, indicative of a shift from perceptually to conceptually-bound processing, and whether any such age-specific profiles are differentially associated with fluid IQ (*Objective 1*). We further tested the adaptiveness of brain-environment alignment by probing its relevance for individual differences in fluid IQ and affectively-driven attentional processing biases (*Objective 2*). Finally, we investigated whether overlapping patterns of functional network integration underlie dynamic brain reconfiguration in response to both high-level narrative context changes and low-level featural fluctuations (e.g., presence/absence of objects, people), thereby linking event segmentation processes unfolding at multiple time scales (*Objective 3*).

This report is organized as follows. Part 1 targets objective 1 in a healthy adult lifespan sample collected by the Cambridge Centre for Ageing and Neuroscience (Cam-Can). Part 2 addresses objectives 2 and 3 in a separate sample of healthy young adults from the Human Connectome Project (HCP).

Part 1: Cam-Can Sample

Results

Window-to-window and narrative context-based brain reorganization increase with age; neither is linked to intelligence beyond age. We ran ten discovery CCAs to characterise the relationship of window-to-window and narrative-based functional reconfiguration with age,

as well as fluid and crystallised intelligence. The discovery CCAs identified one significant mode, which was validated across all test sets (r of .15, $p = 7 * 10^{-5}$). This mode indicated that greater functional brain reconfiguration (i.e., reduced similarity in community structure between temporally adjacent windows, as well as neighbouring windows from distinct narrative segments) typifies older individuals with lower fluid intelligence scores (see Figure 3-a, d). An inspection of the standardized coefficients revealed that the link between greater architectural variability and intelligence is mostly due to age (i.e., older individuals tend to have lower fluid intelligence scores relative to younger individuals, see Figure 3-b, e).

Window-to-window and narrative context-based brain reorganization are linked to distinct patterns of network participation as a function of age. Ten discovery CCAs were conducted to probe the relationship between diversity in the functional interactions of the ten networks from the Power atlas (i.e., the average participation coefficient across all the ROIs within each network) and age-linked patterns of window-to-window versus narrative context-based brain reorganization. The discovery CCAs detected two significant modes, which were validated across all test sets (rs of .50 and .31, respectively, both ps of 10^{-5}). The first mode indicated that, at older ages, functional brain reorganization is associated with greater participation of networks involved in self-guided cognition and creation of situation models during event perception (DMN), as well as top-down control (FPC) and attention (DAN), but reduced participation of networks implicated in environmentally driven processing (CON, AUD, SAL and VAN, see Figure 4). The second mode suggested that, at younger ages, stronger brain reconfiguration was linked to greater global participation, but particularly for the network involved in environmental vigilance and control maintenance (CON, cf. Figure 5).

The network participation profile linked to brain reconfiguration at younger ages, predicts fluid IQ independent of age and beyond levels of window-to-window /context -based reconfiguration; neither network participation profile predicts crystallised IQ. A robust regression analysis, conducted in Matlab with default settings (bisquare robust fitting weight function with a tuning constant of 4.685) and using fluid IQ as the outcome, revealed its significant positive association with the network participation profile linked to brain reconfiguration during, younger (b = .083, SE = .031, $t(602)$ = 2.643, p =.008), but not older (b = -.053, SE = .037, $t(602)$ = -1.433, p =.153), ages (covariates included window-to-window and context-based brain reconfiguration, respectively, age, sex, handedness, crystallised IQ, the summary motion metric and the summary ROI homogeneity metric) (see Figure 6). The corresponding robust regression analysis using crystallised IQ as the outcome unveiled no significant associations with either participation profile (both ps > .66). In neither robust regression analysis did levels of window-to-window or context-based functional reconfiguration made a significant contribution to either fluid or crystallised intelligence (all ps > .25).

A subset of DMN ROIs predicts reconfiguration linked to narrative context boundaries, independent of age and window-to-window reconfiguration level. The behavioral PLS analysis identified one ROI participation LV (p = .0005) which was significantly linked to reorganization in response to movie event boundaries, independent of age and window-to-window brain reconfiguration levels (r = .25, 99% CI= [.25; .45]). Ten ROIs, all but one in the DMN, made a reliable contribution (absolute value BSR > 3) to this LV (insula, angular gyrus [AG], middle temporal gyrus [MTG], posterior cingulate cortex [PCC], superior frontal gyrus [SFG], dorsomedial and ventromedial prefrontal cortex [dmPFC, vmPFC], see Figure 7-a).

Subsequently, we conducted a decoding analysis in Neurosynth (Yarkoni et al., 2011), focused on the central voxel within each of the ROIs robustly linked by PLS to brain reconfiguration in response to event boundaries, in order to shed some light on their previously documented functional associations. As can be seen in Figure 7-b, the analysis revealed that the strongest z-score-based (Neurosynth z-scores > 4) associations were with "memory", "autobiographical", "episodic", "retrieval", "mind" and "remembering". These decoding results are compatible with the interpretation that brain sensitivity to narrative context boundaries is uniquely associated with greater functional integration of ROIs that are relevant to the formation of ongoing event representations and play a key role in internally guided mnemonic processes (Honey, Newman, & Schapiro, 2017; Stawarczyk, Bezdek, & Zacks, 2019).

A subset of DMN, VIS and FPC ROIs predicts window-to-window reconfiguration, independent of age and event boundary-based reconfiguration level. This second behavioural PLS analysis identified one ROI participation LV (p = .0002) which was significantly linked to window-to-window reorganization, independent of age and narrative context-based brain reconfiguration levels (r = .26, 99% CI= [.26; .46]). Nine ROIs, encompassing the DMN (dmPFC, SFG), VIS (fusiform gyrus [FG], inferior occipital gyrus [IOG]), and FPC (inferior parietal lobule [IPL], medial frontal gyrus [MFG]) made a reliable contribution (absolute value BSR > 3) to this LV (see Figure 8-a).

A decoding analysis in Neurosynth, similar to the one conducted for narrative context-based reconfiguration, revealed that the ROIs linked to window-to-window brain reconfiguration showed strongest functional associations with "visual", "memory", "objects", "language", "social", "mind", and "retrieval" (see Figure 8-b). This functional web was quite distinct from the one observed for the ROIs uniquely associated with context-based reconfiguration.

Part 2: HCP Sample

Results

Anxious younger adults with lower fluid IQ show greater brain sensitivity to object-based, but not action-based changes in the external environment. Ten discovery CCAs were conducted to probe the relationship between age, fluid IQ, anxiety and depression, on one hand, and coupling of functional brain reconfiguration with semantic feature (noun vs. verb-based) changes across all 14 movies. The discovery CCAs detected one significant mode, which was validated across all test sets (r of .20, p = .004). This mode indicated that greater functional brain reconfiguration as a function of object-based, but not action-based changes, typifies anxious younger adults with lower fluid IQ scores (see Figure 9).

Greater brain sensitivity to object-based environmental changes is linked to greater whole-brain participation of parietal and medial temporal areas involved in autobiographical and episodic memory. We conducted ten discovery CCAs, probing the link between brain-environment coupling based on object-based variations and participation of the eleven ROIs uniquely linked in the Cam-Can to brain reconfiguration evoked by high-level, narrative context changes. Because we were interested specifically in brain-environment coupling with respect to object-related variations (due to its relevance to cognitive-affective adaptation, as shown in the previous set of CCAs), we regressed out from the brain-index not only global window-to-window brain reconfiguration (as in the prior analysis), but also brain-environment coupling based on narrative action changes. Age was introduced in this analysis to probe whether its link to brain-environment coupling is independent of the narrative ROI participation patterns (in the Cam-Can, the ROI participation profiles were shown to contribute

198 to high-level context-based reconfiguration irrespective of age, but it was unclear whether the
199 same would be true with to lower-level featural fluctuations).

200 One significant mode emerged from the discovery CCAs, which was replicated across all
201 test sets (r of .19, p = .005). This mode indicated that stronger brain-environment coupling (with
202 respect to object-based fluctuations) was associated with greater participation across most of the
203 Cam-Can ROIs at younger ages, but particularly the medial temporal and parietal ROIs, which,
204 based on Neurosynth decoding, were most relevant to "memory", "autographical", "episodic"
205 and "retrieval" (see Figure 10-a,b, d).

206 **Discussion**

207 Extending prior literature on the role of variability in task-evoked brain activation levels
208 (Garrett et al., 2013, 2015, 2020; Grady & Garrett, 2018), we provide novel evidence that the
209 adaptiveness of both spontaneous (i.e., stimulus-independent) and task-related fluctuations in
210 whole-brain functional architecture varies across the lifespan as a function of the underlying
211 network communication profiles. We further demonstrate that in young adulthood, enhanced
212 brain-environment alignment with respect to lower level featural fluctuations, a potential marker
213 of preferential reliance on sensory-bound, rather than more abstract mental representations (cf.
214 Brewin et al., 2010), carries adverse implications for both cognitive and affective adaptation (i.e.,
215 fluid intelligence, depression/anxiety). Finally, we offer suggestive evidence on the network
216 integration profiles that link functional brain reconfiguration at multiple timescales and are, thus,
217 likely to be key to understanding the dynamics behind typical and atypical variations in event
218 processing.

219 Using a naturalistic, dynamic cognition paradigm (i.e., movie watching) in an adult
220 lifespan sample, we demonstrate that the adaptiveness of functional brain reconfiguration hinges

on the associated patterns of whole-brain network participation. Specifically, superior cognitive adaptability (i.e., higher fluid intelligence, Cattell, 1971) was not linked to variability in functional neural architecture per se, but rather to a network participation profile implicated in dynamic brain reconfiguration in younger adulthood. This profile reflects a pattern of whole-brain functional integration anchored in networks implicated in vigilance and control maintenance (CON), as well as environmentally driven attention (VAN) and behavioural regulation (SAL) (see Figure 5-a, Corbetta & Shulman, 2002; Sadaghiani & D'Esposito, 2015; Seeley et al., 2007; Sridharan, Levitin, & Menon, 2008). These results thus dovetail nicely with extant theory which suggests that flexibility in the interactions of cognitive control networks, particularly CON, are a key contributor to fluid intelligence (Barbey, 2018; Duncan et al., 2020). They are also compatible with the interpretation that adaptive patterns of dynamic brain reconfiguration during movie watching are linked to greater whole-brain informational flow through a system implicated in maintaining current task demands (i.e., CON, Dosenbach et al., 2006, 2008) and which is thus very well-positioned to support the "working event model" of an ongoing experience (Radvansky & Zacks, 2017).

In contrast to the participation profile associated with functional reconfiguration in younger adulthood, the one linked to variability in functional architecture during older adulthood was typified by reduced CON, VAN, and SAL participation and, instead, reflected most strongly the diverse interactions of the networks involved in self-guided cognition (DMN) and top-down control (FPC), in particular, but also of those implicated in goal-directed attention (DAN) and visual processing (Andrews-Hanna, Saxe & Yarkoni, 2014; Corbetta et al., 2000; Spreng et al., 2010) (see Figure 4-a). Our finding that functional brain reconfiguration in older adulthood depends on neural communication pathways grounded in the DMN and FPC complements

current theories of cognitive ageing, which posit that age-related declines in the ability to engage strategically with the external environment in the here-and-now are compensated by drawing on accumulated world knowledge (Spreng & Turner, 2019). This age-related semanticisation, which is presumably supported through progressively stronger functional coupling between the DMN and the FPC (Turner & Spreng, 2015), helps preserve task performance in contexts where prior knowledge is relevant (Umanath & Marsh, 2014). One such context may be event segmentation, where it has been suggested that performance preservation with ageing may be partly due to increasing reliance on semantic knowledge (rather than perceptual representations) during event perception (Radvansky & Dijkstra 2007). This conjecture is compatible with recent neuroimaging findings that, with ageing, narrative event boundaries evoke weaker activation in canonical episodic memory areas (but not in areas relevant to more abstract, schematic processing), an effect that emerges despite the lack of age-related differences in behavioural event segmentation (Reagh et al., 2020).

Our present findings thus raise the possibility that the patterns of DMN/FPC participation observed in older adulthood reflect the greater influence of conceptual, rather than perceptual, processes on naturalistic neurocognitive dynamics. Nonetheless, future research incorporating longer movies and behavioural measures of event segmentation is warranted to shed light on how DMN/FPC network communication pathways may contribute to the dynamics of event perception and memory across the lifespan. Further characterisation of the interactions among the internally versus externally oriented DMN and FPC subsystems, respectively (Chiou, Humphreys, & Lambon Ralph, 2020; Dixon et al., 2018), may also provide unique insights into the processes through which rich percepts are translated into transient or more durable mental representations.

Our study also provided novel insights into the adverse functional implications linked to brain-environment entrainment with respect to momentary featural fluctuations. Prior evidence indicates that anxiety and depression are associated with divergent processing biases (i.e., preferential reliance on perceptual versus abstract information), which impact event perception and segmentation (Belzung et al., 2015; Brewin et al., 2010; Petrican et al., 2015; Sherrill et al., 2019). Accordingly, we find that subclinical anxiety is linked to increased brain-environment alignment, compatible with an attentional bias towards lower level featural information (Figure 9-a, b), while an opposite tendency, consistent with attentional disengagement from concrete object representations in the here-and-now, is observed for subclinical depression (Figure 9-e). Brain sensitivity to low-level featural fluctuations was also associated with poorer fluid intelligence. This implies that environmental entrainment, a plausible marker of preferential reliance on sensory-bound, rather than more abstract mental representations, which is linked to high levels of both state and trait anxiety, may prevent successful strategic processing (Hermans et al., 2014; Matthews, Yiend, & Lawrence, 2006; Sylverster et al., 2012).

It is worth pointing out that while brain sensitivity to object/spatial layout fluctuations was associated with adverse outcomes (cf. Brewin et al., 2010), the opposite pattern of results emerged with respect to brain sensitivity to action-based changes (Figure 9-b). This pattern of results is compatible with prior findings that action-related changes make a substantial contribution to behavioural event segmentation, an effect that can be observed from childhood and that is attenuated in anxiety-related disorders (Belayachi & & Van der Linder, 2015; Levine, Buchsbaum, Hirsh-Pasek, & Golinkoff, 2019; Magliano & Zacks, 2011; Swallow, Kemp, & Simsek, 2018). If action-related changes are more informative than object or spatial layout-related changes for understanding story flow, then the greater sensititivity to object-based

changes observed in our study may reflect poor tuning to the current task demands. Although this is a possibility that warrants further investigation, we would like to point out that roughly half of the HCP movies did not have a very strong narrative thread and, in many instances, movie flow depended as much on narrative action as it did on object- and spatial layout-related changes (which rendered both types of changes "task-relevant"). Similarly, as pointed out elsewhere (Reagh et al., 2020), most of the narrative event boundaries in the Cam-Can movie data involved changes in spatial context. Thus, it seems likely that in both datasets, object/spatial layout-related fluctuations were relevant to event segmentation processes. Nonetheless, future studies are needed to further explore the distinct roles that brain sensitivity to changes in object and/or spatial layout versus action flow may play in encoding and subsequently retrieving perceptually rich event representations.

Our study also contributed novel evidence on the overlapping network communication profiles underlying brain-environment alignment with respect to both higher-level contextual and lower-level featural fluctuations (as outlined above though, note that in the present data featural fluctuations relevant to spatial layout were relevant to higher level event boundaries, cf. Reagh et al., 2020). In both cases, brain-environment coupling was associated with greater whole-brain informational flow (i.e., participation) in a subset of canonical DMN ROIs, including the left AG, left MTG, PCC and left SFG, the majority of which had been implicated in event memory reactivation (Chen et al., 2017), a finding that resonates with our Neurosynth decoding results (Figure 10-d). The AG and PCC play key roles in recollection (Ranganath & Ritchey, 2012; Ritchey & Cooper, 2020; Rugg & Vilberg, 2013) and have been widely implicated in the integration of multimodal information at longer timescales, thereby supporting the creation of the so-called "situation/event models"(Bonnici, Richter, Yazar, & Simmons, 2016; Chen et al.,

2016; Hasson, Chen, & Honey, 2015; Radvansky & Zacks, 2017; Stawarcyzk et al., 2019; Yazar, Bergstrom, & Simmons, 2017). The left AG, in particular, has been posited to play a causal role in episodic context creation during perception by acting as an online buffer for combining past and currently presented information (Branzi, Pobric, Jung, & Lambon Ralph, 2019; Humphreys & Lambon Ralph, 2015). Our study expands the literature on AG by documenting its role in integrating information across the whole brain during event perception in order to align the external environmental and internal neural dynamics. It also raises the possibility that, through its contribution to unifying information processing across multiple levels (i.e., from featural to contextual), the AG may play a critical role in setting attentional focus, thereby shifting from a featural, sensory-bound to a more abstract processing mode in a context-specific manner. It thus seems likely that the AG would contribute to cognitive adaptability (i.e., fluid IQ), together with "multiple demand" cognitive control areas (Barbey, 2018; Duncan et al., 2020), a proposal that awaits actual testing.

Together with the AG, the left MTG demonstrated a similarly robust association with functional brain reconfiguration triggered by both high and low-level environmental changes. Like AG, this region has been previously implicated in updating semantic features related to the present context (Branzi, Humphreys, Hoffman, & Lambon Ralph, 2020), while uniquely partaking into the controlled retrieval of semantic information (Hoffman, McClelland, & Lambon-Ralph, 2018). Here, it is plausible that the MTG and AG make complementary contributions during online context creation and updating, as pertinent to real-life cognition and our movie watching paradigm (Kurby & Zacks, 2008). Specifically, the whole-brain participation profile associated with AG may provide the low-level, episodic perceptual detail from which a strong sense of perceptual vividness and grounding in the here-and-now stem

(Ramanan, Piguet, & Irish, 2018). Complementarily, during event perception, the MTG-linked participation profile may support continual updating of the underlying semantic structure based on the influx of environmental information and controlled retrieval of already stored world knowledge, thereby playing a critical role in keeping the "working event model" in sync with the ongoing experience (Hoffmann et al., 2018; Zacks, 2020). Following this train of thought, an interesting future research venue would be to probe whether relative expression of the AG- versus the MTG-, linked network communication profile may predict individual differences in preferential reliance on sensory-bound versus more abstract mental representations (cf. Brewin et al., 2010) and, thus, differential vulnerability to anxious versus depressive symptomatology (Belzung et al., 2015; Sherrill et al., 2019).

Future studies are warranted to address limitations of our present research. First, use of a larger battery of movies (as in HCP), covering diverse artistic interests and production dates, with a strong narrative plot that allows reliable extraction of narrative event boundaries (as in Cam-Can), is needed to characterise event perception dynamics at multiple levels of meaning within a single process model. Second, inclusion of a full lifespan sample, as well as complementary cross-sectional/longitudinal designs may elucidate the role of brain-environment entrainment during developmental stages characterised by distinct learning needs (Baldwin & Kosie, 2020). Third, although behavioural event segmentation is largely preserved in healthy ageing (Kurby & Zacks, 2018; Reagh et al., 2020; Sargent et al., 2013), future studies probing the link between event segmentation performance and its neural substrates across the lifespan would be critical in furthering our understanding of developmental differences in information processing. Fourth, research employing alternate methods for estimating dynamic brain

358 reconfiguration, including data-driven approaches, would shed light on the boundary conditions
359 of the effects herein documented (Gonzalez-Castillo & Bandettini, 2018; Iraji et al., 2020).
360 In sum, we demonstrate that the adaptiveness of dynamic brain reconfiguration varies
361 across the lifespan based on the associated patterns of network interaction. We also show that
362 brain-environment alignment at the level of momentary featural fluctuations, a potential indicator
363 of the predisposition to rely on lower-level, sensory, rather than higher-level, more abstract
364 mental representations (cf. Brewin et al., 2010), carries adverse implications not only for
365 affective adjustment, but also for the capacity to cognitively adapt to novel environments.
366 Finally, we provide evidence that brain sensitivity to lower level featural fluctuations is higher in
367 younger adulthood and is associated with some of the network interaction profiles that typify
368 sensitivity to higher level narrative event boundaries across the lifespan. These network
369 communication profiles, which link event segmentation at multiple levels during earlier life, are
370 relevant to the provision of perceptual and semantic scaffolding to context formation during
371 perception, as well as during the subsequent episodic retrieval of these event representations.

Methods

Part 1: Cam-Can Sample

Participants. We included the largest number of participants from Stage II of the Cambridge Ageing and Neuroscience (Cam-Can) study with available fMRI data in the movie watching condition (N = 642, age range: 18-88 yrs [M = 54 yrs, SD = 19 yrs]).

The majority of participants (N = 589) were predominantly right-handed (handedness measure > 0). The sample included 316 men (32 between 18 and 29, 49 between 30 and 39, 48 between 40 and 49, 48 between 50 and 59, 57 between 60 and 69 , 50 between 70 and 79, 32 between 80 and 88 years of age) and 326 women (42 between 18 and 29, 46 between 30 and 39, 57 between 40 and 49, 45 between 50 and 59, 48 between 60 and 69 , 58 between 70 and 79, 30 between 80 and 88 years of age).

All participants were cognitively healthy (MMSE > 24) and met the hearing, vision, and English language ability criteria necessary for the completing experimental tasks (Taylor et al., 2017). They were also screened for any neurological and serious psychiatric conditions, as well as for physical conditions or bodily implants that may render their participation unsafe (Taylor et al., 2017). Participants provided informed consent in accordance with the Cambridgeshire research ethics board (Shafto et al., 2014).

Out-of-scanner measures.

Fluid intelligence. Participants completed the pen-and-paper version of the Cattell Culture Fair Test, Scale 2 Form A (Cattell, 1971; Cattell & Cattell, 1973) in which they had to select the correct answer from multiple alternatives and record it on an answer sheet. The test contains four subtests with distinct non-verbal “puzzles”: series completion, classification, matrices and conditions. Unbeknownst to the participants, each subtest is timed, such that 3, 4, 3

and 2.5 minutes are allocated for subtest 1, 2, 3 and 4, respectively. Correct responses receive a score of 1 for a maximum score of 46.

Crystallized intelligence. The proverb comprehension test was used as an index of crystalized intelligence (Crawford & Stankov, 1996). In this task, participants provide the meaning of three common proverbs in English, which are presented on a computer screen (Shafto et al., 2014). Their responses are recorded digitally and scored by experimenters as incorrect or a "don't know" response (0), partly correct but literal rather than abstract (1), or fully correct and abstract (2). The highest possible score is 6.

In-scanner task. Participants watched a shortened version of Alfred Hitchcock's black-and-white television drama "Bang! You're Dead" (Hitchcock, 1961; Hasson et al., 2008, 2010) edited from 30 min to 8 min while maintaining the plot (Shafto et al., 2014). The movie was selected to be engaging and unfamiliar to the participants.

fMRI data acquisition. Images were acquired with a 3T Siemens TIM Trio System (32-channel coil). T1-weighted anatomical scans were acquired with a MPRAGE sequence (TR = 2250 ms, TE = 2.99 ms, flip angle=9°, FOV = 256 mm x 240 mm x 192 mm, 1 mm isotropic voxels, GRAPPA acceleration factor = 2). Functional images were acquired with a multi-echo EPI sequence (TR=2470 ms, [TE=9.4 ms, 21.2 ms, 33 ms, 45 ms, 57 ms], flip angle=78°, FOV = 192 x 192 mm, 32 axial slices of 3.7 mm thickness, acquired in descending order with 20% gap, voxel size of 3 mm × 3 mm x 4.4 mm).

fMRI data preprocessing. The main preprocessing and analysis steps for both samples are presented in Figure 1. For the Cam-Can data, preprocessing began with the averaging of the corresponding images from the multiple echos. We opted for a simple average, rather than a weighted sum, in order to maximize comparability with the HCP data, which did not contain

multiple echos. We reasoned that our strategy was defensible in light of evidence that simple averaging yields similar improvements in 3T image quality as weighted summing (Kettinger et al., 2016; Poser, Versluis, Hoogduin, & Norris, 2006). Subsequently, we performed image processing in SPM12 (Wellcome Department of Imaging Neuroscience, London, UK). Specifically, we corrected for slice timing differences and rigid body motion (which included unwarping), spatially normalized the images to the standard Montreal Neurological Institute (MNI)-152 template, and smoothed them (full-width half-maximum, 6 mm).

Additional denoising. Because motion can significantly impact functional connectivity measures (Power et al., 2012; Van Dijk et al., 2012), we implemented several additional preprocessing steps to address this potential confound. First, after extracting the BOLD time series from our regions-of-interest (ROIs, see below), but prior to computing the ROI-to-ROI correlations, we used the Denoising step in the CONN toolbox (version 17c; Whitfield-Gabrieli & Nieto-Castanon, 2012) to apply further physiological and rigid motion corrections. Specifically, linear regression was used to remove from the BOLD time series of each ROI the BOLD time series of the voxels within the MNI-152 white matter and CSF masks, respectively (i.e., the default CONN option of five CompCor-extracted principal components for each, Behzadi, Restom, Liau, & Liu, 2007), the 6 realignment parameters, their first-order temporal derivatives and their associated quadratic terms (24 regressors in total, cf. Bolt et al., 2017). The residual BOLD time series were bandpass filtered ($0.008\ Hz < f < 0.09\ Hz$), linearly detrended and despiked (all three are default CONN denoising steps). Following these corrections (which did not include global signal regression) (Murphy & Fox, 2017), an inspection of each subject's histogram of voxel-to-voxel connectivity values revealed a normal distribution, approximately centered around zero, which would suggest reduced contamination from physiological and

441 motion-related confounds (cf. Whietfield-Gabrieli & Castanon, 2012). Nonetheless, in all
442 hypothesis testing analyses, we controlled for the average relative (i.e., volume-to-volume)
443 displacement per participant, a widely used motion metric (Power et al., 2012, 2015;
444 Satterthwaite et al., 2013).

445 **fMRI data analysis.**

446 ***ROI time series.*** 229 nodes for 10 core large-scale functional brain networks (i.e.,
447 default-mode [DMN], frontoparietal [FPC], cingulo-opercular [CON], salience [SAL], dorsal
448 attention [DAN], ventral attention [VAN], somatomotor [SM], subcortical [SUB], auditory
449 [AUD] and visual [VIS]) were defined for each participant as spherical ROIs (radius 5 mm)
450 centered on the coordinates of the regions reported in Power et al. (2011) and assigned network
451 labels corresponding to the graph analyses from this earlier article. We selected the Power et al.
452 atlas because it was created by taking into account both the task-related activation (derived meta-
453 analytically) and the resting state connectivity patterns of the component voxels for each ROI.
454 Thus, this atlas provided an optimal parcellation scheme for charactering functional brain
455 reorganization during a naturalistic cognition condition that, due to the lack of an explicit task,
456 was likely to share significant similarities with a resting state condition (Vanderwal et al., 2017).
457 The ROIs were created in FSL (Smith et al., 2004), using its standard 2 mm isotropic
458 space, with each ROI containing 81 voxels. These template space dimensions were selected
459 because they yielded the most adequate spatial representation of the Power atlas. The 229 ROIs
460 represent a subset of the 264 putative functional areas proposed by Power et al. (2011). The 229
461 ROIs were selected because, based on Power et al.'s analyses, they showed relatively
462 unambiguous membership to one of the ten large-scale functional networks outlined above.

Fit of the Power atlas to the present dataset. To evaluate the homogeneity of the Power ROIs across the Cam-Can adult lifespan sample (cf. Iraji et al., 2020), we used an approach that is conceptually similar to those recently used in the literature (Gordon et al., 2016; Siegel et al., 2016). Specifically, we used the CONN toolbox to compute the radial similarity contrast (RSC) for each voxel in the Power atlas. As implemented in CONN, the RSC reflects the amount of similarity in whole brain connectivity patterns between a voxel and its neighbours in each of the three space directions (x,y,z), and is thus a 3 dimensional construct (see also Kim et al., 2010). If a node is functionally homogenous, then the RSC of its voxels should be relatively similar (i.e., across the entire ROI, there should be a consistent degree of similarity among the component voxels' whole brain connectivity patterns). To test this hypothesis, for each participant, we conducted a principal components analysis of the RSC of the 81 voxels within each ROI (i.e., for each participant, one ROI constituted one case, whereas the RSC of one voxel within a given ROI constituted a variable). As a measure of similarity among the RSC of all voxels within a node across all nodes, we took the percent of variance explained by the first component extracted through the analysis just described (see also Gordon et al., 2016; Siegel et al., 2016). Because, as previously mentioned, RSC is a three-dimensional vector, this set of analyses yielded, for each participant, three indices of average similarity in global functional connectivity patterns among all voxels within a given ROI. The three indices were significantly positively correlated across participants (Spearman's *rho*s from .17 to .24, all *p*s < .0001), which is why we averaged them to create a summary measure of ROI functional homogeneity. A correlational analysis, based on 100,000 permutation samples, revealed a modest, but significant negative relationship between age and the average similarity in global functional connectivity patterns among the component voxels of the Power ROIs (Spearman's *rho* of -.21, $p = 10^{-5}$). As expected, given that the Power

ROIs were validated on a sample corresponding in age to the first decade of the Cam-Can sample, a second robust regression analysis revealed no evidence of significant quadratic age effects on the functional homogeneity of the Power ROIs ($p > 0.56$). Based on these results, the summary measure of ROI functional homogeneity was introduced as a covariate in all hypothesis testing analyses.

Fit of the Power network assignment to the present dataset. To estimate the fit of Power et al.'s (2011) network assignments to the present data, we used the same algorithm utilized by these authors for community detection, i.e., Infomap (Lancichinetti & Fortunato, 2009; Rosvall & Berstrom, 2008). We ran our analyses using Infomap Online (D. Edler & M. Rosvall) available at www.mapequation.org/infomap.

Following Power et al. (2011), we conducted all our community detection analyses on group-averaged ROI-to-ROI correlation matrices. To test whether Power et al.'s (2011) network assignments provide an equally adequate fit to the present connectivity data across the lifespan, we first averaged the individuals' ROI-to-ROI correlation matrices, obtained from CONN, separately within each of the seven decades. Next, we used the Brain Connectivity Toolbox (BCT, Rubinov & Sporns, 2010) to threshold each of the seven matrices at the same tie densities used by Power et al. (2011) for the areal graph (i.e., 2% to 10% tie density in increments of 1%). BCT was subsequently utilized to write the thresholded matrices into a Pajek *.net format and the resulting files were inputted into Infomap. Infomap was run with the option of extracting a one-level structure (i.e., no nested modules), which is the format of Power et al.'s (2011) atlas as is publicly available. Finally, we used again the BCT to compute the normalized mutual information index (NMI; range: 1 [perfect similarity] to 0 [no similarity at all]) as a measure of similarity between Power et al.'s network assignments and those outputted by Infomap for the

connectivity data from each of the Cam-Can's seven decades (Fornito, Zalesky & Bullmore, 2016). As can be seen in Figure 2, across all tie densities, the network structure from each of the seven age groups exhibited equivalent levels of similarity with that proposed by Power et al. (2011). These results thus suggest that Power et al.'s network structure provide an adequate fit to the present connectivity data across the lifespan (i.e., the NMI values were similar to those documented by Power et al. when comparing network structure across cohorts).

Functional connectivity analyses. Pairwise coupling among the 229 ROIs was estimated in CONN. Pairwise correlations among all the ROIs were expressed as Fisher's z-scores. Consistent with existing practices aimed at maximizing interpretability of results in network neuroscience studies of individual or group differences (e.g., sex or age, Betzel et al., 2014; Satterthwaite et al., 2015), we used both positive and negative z-scores to compute the indices of interest for all connectivity analyses. We reasoned that such an approach would be particularly well-justified in our present case since global signal regression, an artefact removal technique that generates negative correlations whose interpretation is still controversial, was not part of our preprocessing pipeline (for further discussion on the validity of the negative correlations obtained with the CONN toolbox, see Whitfield-Gabrieli & Nieto-Castanon, 2012).

To characterize individual differences in dynamic network structure, we used a combined window and clustering based approach (Iraji et al., 2020; Lurie et al., 2020). Thus, we broke down the movie into partially overlapping 40 s long windows for a total of 177 windows. This window length was selected in light of prior evidence that it both maximizes detection of individual differences in dynamic network reconfiguration and enables identification of a stable functional core (Leonardi & Van De Ville, 2015; Preti, Bolton, de Ville, 2017; Telesford et al., 2016; for similar window sizes in dynamic connectivity analyses of HCP data, see also Chen et

al., 2016). Thus, pairwise coupling among the 229 ROIs was estimated in CONN using a sliding window of 40 s in length (~ 16 volumes), with one TR (2.47 s) gap and a "hanning weighting" (i.e., greater weight to the scans in the middle of the window relative to the ones at the periphery) applied to all the time points within a window. The use of a hanning weighting was intended to reduce the autocorrelation in the fMRI data series and, thus, maximize the opportunity to detect differences in functional brain organization between adjacent windows.

Network-level analyses. All the network-level metrics were computed using the Brain Connectivity Toolbox (BCT, Rubinov & Sporns, 2010) and the Network Community Toolbox (Bassett, D.S. [2017, November]. Network Community Toolbox. Retrieved from http://commdetect.weebly.com/), as described below.

Community detection. Rather than being computed directly, the degree to which a network can be fragmented into well-delineated and non-overlapping communities or modules is estimated using optimization algorithms, which sacrifice some degree of accuracy for processing speed (Fornito et al., 2016; Rubinov & Sporns, 2010). Here, the optimal whole-brain division into constituent communities was estimated using a Louvain community detection algorithm implemented in the BCT. This algorithm partitions a network into non-overlapping groups of nodes with the goal of maximizing an objective modularity quality function, Q (Betzel & Bassett, 2017; Rubinov & Sporns, 2011; Sporns & Betzel, 2016). There are multiple strategies for estimating community structure based on sliding window data, as was the case of our movie viewing data. Specifically, multilayer modularity algorithms (Bassett et al., 2011; Braun et al., 2015; Mucha et al., 2010) can provide important insights into community dynamics at multiple time scales. Nonetheless, such algorithms require estimation of additional free parameters (e.g., the temporal coupling parameter between two adjacent temporal windows). Since we feared that

555 estimation of the temporal coupling parameter could act as a potential confound when comparing
556 connectivity results across the multiple samples included in the analysis, we used the same
557 procedure to estimate community structure independently in each sliding window (see also Chen
558 et al., 2016), as described below.

559 For signed networks, such as the ones investigated in our study, optimization of the Q
560 function can be achieved by either placing equal weight on maximizing positive within-module
561 connections and minimizing negative within-module connections or by putting a premium on
562 maximizing positive connections, which have been argued to be of greater biological
563 significance (Fornito et al., 2016; Rubinov & Sporns, 2011). Although we verified that all the
564 reported results emerge with either formula, for the sake of simplicity and because we agree with
565 their argument regarding the greater importance of positive weights in determining node
566 grouping into communities, we report here the results based on Rubinov and Sporns's modularity
567 formula (cf. Chen et al., 2016; Rubinov & Sporns, 2011). In this formulation, the contribution of
568 positive weights to Q is not affected by the presence of negative weights in the network, whereas
569 the contribution of negative weights to Q decreases with an increase in positive weights.

570 The adapted modularity function Q^*, proposed by Rubinov and Sporns (2011) is written
571 as

572 $$Q^* = \frac{1}{v^+}\sum_{ij}(w^+_{ij} - \gamma e^+_{ij})\delta_{M_iM_j} - \frac{1}{v^+ + v^-}\sum_{ij}(w_{ij}{}^- - \gamma e^-_{ij})\delta_{M_iM_j},$$

573 where $\delta_{MiMj} = 1$ if nodes i and j are in the same module and $\delta_{MiMj} = 0$ otherwise; v^+ and v^-
574 constitute the sum of all positive (w^+) and all negative (w^-) weights in the network, respectively;
575 $w^{\pm}_{ij}$ represent the actual within-module positive or negative connection weights with $w^{\pm} \in (0,1]$;
576 γ is a resolution parameter determining the size of the identified modules; $e^{\pm}_{ij}$ is the within-
577 module connection strength expected by chance and defined, for each node-to-node (i,j)

connection as $e^{\pm}_{ij} = \frac{s_i^{\pm} s_j^{\pm}}{v^{\pm}}$, with $s^{\pm}_i$ and $s^{\pm}_j$ being the sum of all positive or all negative connection weights of node i and j, respectively, while $v^{\pm}$ is the sum of all positive or all negative connection weights in the network.

To account for the near degeneracy of the modularity landscape (i.e., many near-optimal ways of partitioning a network into non-overlapping communities, Good et al., 2010) and for changes in community structure due to variations in the estimation parameters, the community detection algorithm was each initiated 100 times for three values of the spatial resolution parameter, centered around the default value of 1 (cf. Betzel & Bassett, 2017; Braun et al., 2015; Chen et al., 2016). Based on the results of these analyses, run separately for each of the three spatial resolution values, a consensus partition (i.e., whole-brain division into constituent communities) was estimated for each participant in each movie window (cf. Bassett et al., 2013; Lancichinetti & Fortunato, 2012).

Functional brain reorganization: Window-to-window versus context-based. Using the Network Community Toolbox, we estimated similarity in functional brain organization (i.e., community structure derived with the Louvain algorithm, as described above) between consecutive windows based on the adjusted normalized mutual information index [AMI], corrected for chance (Vinh, Epps, & Bailey, 2010). An index of window-to-window functional brain reorganization was computed by subtracting from 1 the average AMI across all pairs of temporally adjacent windows. This index combines spontaneous (i.e., stimulus-independent) window-to-window functional reconfiguration with reconfiguration driven by low-level, window-to-window perceptual fluctuations (e.g., presence/absence of objects, people).

Employing the event boundaries identified by independent raters in Ben-Yakov and Henson (2018) with a keypress when they felt that "one event [meaningful unit] ended and

another began", we selected pairs of non-overlapping 40 s windows, separated by ~ 5 to 7 s, which belonged to adjacent narrative segments (12 windows in total). Functional brain reorganization in response to high-level narrative context boundaries was estimated by subtracting from 1 the average AMI across all such pairs of temporally adjacent windows. This index reflects functional reconfiguration related to event boundaries, as well as stimulus-independent and lower-level reconfiguration indicative of featural changes (e.g., presence/absence of objects, people).

Network-based diversity in functional interactions. The participation coefficient assesses the diversity of a node's intermodular connections (i.e., the extent to which a node interacts with nodes outside its native community) (Chen et al., 2016; Rubinov & Sporns, 2010). Here, a node's native community was the one to which it was assigned in Power et al. (2011), the study that validated the functional atlas. It is worth pointing out that because our participation coefficient is based on a static community structure, it is not subject to the drawbacks associated with the participation coefficients derived from temporally varying communities (Thompson et al., 2020).

A node's participation coefficient was based on the consensus partitions corresponding to each of the 177 sliding windows and was given by the formula

$$P_i = 1 - \sum_{m \in M} \left(\frac{k_i(m)}{k_i}\right)^2, \text{ where}$$

P_i is the participation coefficient of node i, M is the set of communities from a given partition (in our case, the whole-brain partition into communities, as described by Power et al. [2011]), $k_i(m)$ corresponds to the number of times that node i and all the nodes in community m have been assigned to the same community across all time windows, and k_i is the number of times that node i and the remaining 228 nodes have been assigned to the same community across

all time windows. In our case, higher participation coefficients characterised nodes that tended to show an equal number of interactions (where interaction means assignment to the same community within a sliding window) with nodes from all the functional networks identified by Power et al.

Brain-behavior analyses

Canonical correlation analysis (CCA). To characterize the relationship between functional brain reorganization (i.e., changes in community structure) and network-level diversity in functional interactions, we used canonical correlation analysis (CCA, Hotelling, 1936) with cross-validation procedures (cf. Hair et al., 2008). CCA is a multivariate technique, which seeks maximal correlations between two sets of variables by creating linear combinations (i.e., canonical variates) from the variables within each set. Recently, CCA has been successfully used to investigate brain-behavior relationships in large datasets (see Smith et al., 2015; Tsvetanov et al., 2016; Wang et al. 2020). CCA was implemented in Matlab using the canoncorr module. In order to obtain reliable estimates of correlations between the brain or behavioral variables and their corresponding variates, it is generally recommended that CCA be performed on a sample size at least ten times the number of variables in the analysis (Hair, Anderson, Tatham, & Black, 1998), a criterion which was exceeded in all analyses reported below.

The performance of our CCA-derived models was tested by using a 10-fold cross validation procedure. Specifically, in the CCAs involving age, network participation and functional brain reconfiguration, the data were broken down into ten folds, all but two containing 64 participants for a total of 642 participants. For the CCAs involving fluid and crystallised intelligence, all but three of the ten folds of testing data contained 61 participants for a total of 613 participants. For both sets of CCAs, discovery analyses were conducted on nine folds of data

and the resulting CCA weights were employed to derive predicted values of the brain and behavioral variate in the left-out ("test") fold. This procedure was repeated until each of the ten folds served as "test" data once. The correlation between the predicted brain and behavioral variates across all testing folds was evaluated using a permutation test with 100,000 samples (cf. Smith et al., 2015).

To describe the relationship between the behavioral or brain variables and their corresponding variates across all the testing folds, we include correlations between the observed value of a brain or behavioral variable and the predicted value of its corresponding variate, as well as standardized coefficients, analogous to multiple regression coefficients, which indicate the unique association between the observed value of a behavioral or brain variable and the predicted value of its corresponding variate. For each of the two sets of CCAs, when evaluating the relationship between the predicted values of the two variates or the relationship between the actual value of each variable and the predicted value of its corresponding variate, we controlled for gender, handedness, subject-specific motion and subject-specific ROI functional homogeneity (RSC). 95% confidence intervals (CI) for each correlation and standardized regression-like coefficient were obtained by using the bootci function in Matlab (with default settings and 100,000 bootstrap samples).

The correlation and standardized regression-like coefficients described above are analogous to canonical loadings and canonical weights, respectively (see also Tsvetanov et al., 2016; Vatansever et al., 2017), with the only difference being that they are computed in the test, rather than the discovery, folds and, thus, reflect more conservative effect estimates.

Partial least squares analysis (PLS). To identify patterns of ROI community participation that are specific to functional brain reorganization related to low-level featural

versus high-level contextual changes/narrative event boundaries, we used partial least squares correlation often referred to as *PLS* (Krishnan et al., 2011), a multivariate technique that can identify in an unconstrained, data-driven manner, neural patterns (i.e., latent variables or LVs) related to individual differences variables (behavioral PLS). PLS was implemented using a series of Matlab scripts, which are available for download at https://www.rotman-baycrest.on.ca/index.php?section=345. In the behavioral PLS analyses we conducted, one matrix comprised residual scores on functional brain reorganization linked to event boundaries (i.e., average [1- AMI] across all neighbouring windows from different narrative segments from which age and average window-to-window functional brain reorganization were partialled out) (PLS 1) or average window-to-window functional brain reorganization (i.e., average [1- AMI] across all temporally adjacent windows from which age and average functional brain reorganization linked to event boundaries were partialled out) (PLS 2), whereas the second matrix contained each participant's ROI participation matrices (Krishnan et al., 2011). Each matrix entry corresponded to the participation coefficient of one ROI from one subject.

In all the reported analyses, the significance of each LV was determined using a permutation test with 100000 permutations (in the permutation test, the rows of the ROI participation data are randomly reordered, Krishnan et al., 2011). In the case of our present analyses, PLS assigned to each ROI a weight, which reflected the respective ROI's contribution to a specific LV. The reliability of each ROI's contribution to a particular LV was tested by submitting all weights to a bootstrap estimation (100000 bootstraps) of the standard errors (SEs, Efron, 1981) (the bootstrap samples were obtained by sampling with replacement from the participants, Krishnan et al., 2011). We opted to use 100000 permutations and 100000 bootstrap samples (the same value used for the other bootstrapping and permutation-based testing herein

reported) in order to increase the stability of the reported results, since these parameters are several orders greater than the standard ones (i.e., 500 permutations/100 bootstrap samples), recommended by McIntosh and Lobaugh (2004) for use in PLS analyses of neuroimaging data. A bootstrap ratio (BSR) (weight/SE) of at least 3 in absolute value was used as a threshold for identifying those ROIs that made a significant contribution to the identified LVs. The BSR is analogous to a z-score, so an absolute value greater than 2 is thought to make a reliable contribution to the LV (Krishnan et al., 2011), although for neuroimaging data BSR absolute values greater than 3 tend to be used (McIntosh & Lobaugh, 2004).

Part 2: HCP Sample

Participants. This sample included 176 unrelated participants, whose data had been released as part of the HCP 1200 subjects data package in March 2017. This sample represented the largest number of participants from the HCP 1200 subjects data release who were unrelated to one another and who had available data on all the demographic, behavioral and fMRI assessments of interest.

The majority of participants (N = 163) were right-handed. The sample included 70 younger men (21 between 22 and 25, 35 between 26 and 30, and 14 between 31 and 36 years of age) and 106 younger women (1 between 22 and 25, 49 between 26 and 30, and 56 between 31 and 36 years of age). Although age is presented here in the range format, as advocated by the HCP team (see Van Essen et al., 2012 for the rationale behind this age reporting strategy in HCP data releases), all our brain-behavior analyses used participants' actual age in years, as available in the HCP restricted data release.

All participants were screened for a history of neurological and psychiatric conditions and use of psychotropic drugs, as well as for physical conditions or bodily implants that may

716 render their participation unsafe. Diagnosis with a mental health disorder and structural
717 abnormalities, as revealed by the MRI structural scans, were also exclusion criteria. Participants
718 provided informed consent in accordance with the HCP research ethics board.

719 **Out-of-scanner measures.**

720 ***Fluid IQ.*** Form A of an abbreviated measure of the Raven's Progressive Matrices (RPM;
721 Bilker et al., 2012), a non-NIH Toolbox measure, gauged participants' abstract reasoning skills
722 (i.e., nonverbal fluid IQ). This task features patterns made up of 2x2, 3x3 or 1x5 arrangements of
723 squares, with one of the squares missing. Participants must select one of five response choices
724 that best fits the missing square on the pattern. The task has 24 items and 3 bonus items, arranged
725 in order of increasing difficulty. The task is stopped though if the participant makes 5
726 consecutive incorrect responses. In line with existing guidelines (Bilker et al., 2012; Gray,
727 Chabris, & Braver, 2003; Gray et al., 2005), total number of correct responses was used as a
728 measure of abstract reasoning.

729 ***Subclinical depression and anxiety.*** To assess relatively stable subclinical variations in
730 depression and anxiety, we used participants' scores on the DSM-oriented depression and anxiety
731 scales (see below for details). Both sets of scores were derived from participants' responses to
732 relevant items on the Achenbach Adult Self-Report (ASR) instrument for ages 18–59
733 (Achenbach, 2009). The ASR contains a total of 123 statements relevant to psychological
734 functioning and requires participants to rate on a 3-point scale (0 *not true*, 1 somewhat or
735 sometimes true, 2 *very true or often true*) how well each item described them over the previous
736 six months. The DSM-oriented depression scale includes items such as "I am unhappy, sad, or
737 depressed". The DSM-oriented anxiety scale includes items such as " I worry about my future".

738 **Out-of-scanner control measures.**

Current negative emotion experience. Participants completed the NIH Toolbox Negative Affect Survey, which assesses separately current levels of experienced sadness (e.g., "I felt sad.", "I felt like a failure."), anger (e.g., "I felt angry.", "I felt bitter about things."), and fear (e.g., "I felt frightened.', "I had a racing or pounding heart."), respectively. The measure requires participants to rate on a 5-point scale (1 *never* to 5 *always*) how often they experienced the relevant emotion within the past seven days. Scores on the sadness, anger and fear subscales were averaged to create an index of current negative emotional state, which was entered as a covariate in all the hypothesis testing analyses.

In-scanner task. Participants completed four movie viewing runs over two scanning sessions on two separate days. Each run was about 15 minutes long and comprised 1 to 4.3 minutes long excerpts from Hollywood movies, as prepared and published by Cutting, Brunick, and Candan (2012), and independent films, freely available under Creative Commons Licensing. All four movie runs include a Vimeo repeat clip at the end, which was not included in the analyses. In each run, 20 s of rest (i.e., black screen with "REST" in white text) precede the beginning and follow the end of each movie clip.

Movie features. To quantify low-level featural fluctuations in the movie task, we used the output of the semantic feature coding conducted by Jack Gallant's laboratory (cf. Huth, Nishimoto, Vu, & Gallant, 2012) and available as part of the HCP1200 Subjects Data Release. By using this semantic feature coding, we were able to characterise the extent to which window-to-window reconfiguration in functional architecture is yoked to ongoing, meaningful fluctuations in the external environment. Each movie frame is coded for the presence/absence (0/1) of 859 semantic elements recorded as nouns (N = 629), verbs (N = 229) and adjective(s) (N =1). Our analyses focused on semantic features listed as nouns, which we took to reflect

762 environmental attributes (e.g., presence of objects, people, buildings) and semantic features listed
763 as verbs, which reflected actions performed by the movie characters or natural phenomena. As
764 we detail below, the brain data corresponding to each movie was broken down into 40 s second
765 sliding windows, moved in increments of 2 s. The binary semantic feature matrices
766 corresponding to each sliding window from the brain data were averaged. In these averaged
767 matrices, the value in each cell signified the percentage of frames within a sliding window when
768 an entitity or action was present. As in the brain data, window-to-window similarity in semantic
769 features was indexed with the adjusted mutual information index (AMI) (Vinh et al., 2012), with
770 each unique value in the averaged semantic features for each window acting as a community
771 label.

772 **fMRI data acquisition.** Images were acquired with a customized Siemens 3T
773 "Connectome Skyra" scanner housed at Washington University in St. Louis (32-channel coil).
774 Pulse and respiration were measured during scanning. Functional images were acquired with a
775 multiband EPI sequence (TR=1000 ms, TE=22.2 ms, flip angle=45°, FOV = 208 x 208 mm, 85
776 slices of 1.6 × 1.6 mm in-plane resolution, 1.6 mm thick, no gap). Two of the movie runs were
777 acquired with an anterior-to-posterior, while the other two with a posterior-to-anterior, phase
778 encoding sequence (so that phase encoding sequence effects could cancel each other out over the
779 all runs).

780 **fMRI data preprocessing.** The present report used the minimally preprocessed movie
781 watching data from the HCP 1200 subjects data release. These data have been preprocessed with
782 version 3 of the HCP spatial and temporal pipelines (Smith et al., 2013; for specification of
783 preprocessing pipeline version, see http://www.humanconnectome.org/data). Spatial
784 preprocessing involved removal of spatial and gradient distortions, correction for participant

785 movement, bias field removal, spatial normalization to the standard Montreal Neurological
786 Institute (MNI)-152 template (2 mm isotropic voxels), intensity normalization to a global mean
787 and masking out of non-brain voxels. Subsequent temporal preprocessing steps involved weak
788 high-pass temporal filtering with the goal of removing linear trends in the data.

789 ***Additional denoising***. Because motion can significantly impact functional connectivity
790 measures (Power et al., 2012; Van Dijk et al., 2012), we implemented the same additional
791 preprocessing steps used to address this potential confound in the Cam-Can data. Specifically, in
792 the CONN toolbox (version 17c; Whitfield-Gabrieli & Nieto-Castanon, 2012), linear regression
793 was used to remove from the BOLD time series of each ROI the BOLD time series of the voxels
794 within the MNI-152 white matter and CSF masks, respectively (i.e., the default CONN option of
795 five CompCor-extracted principal components for each, Behzadi, Restom, Liau, & Liu, 2007),
796 the 6 realignment parameters, their first-order temporal derivatives and their associated quadratic
797 terms (24 regressors in total, cf. Bolt et al., 2017), as well as the main movie effects, obtained by
798 convolving a boxcar task design function with the hemodynamic response function, and their
799 first temporal order derivative (cf. Braun et al., 2015; Vatansever et al., 2015; Westphal, Wang,
800 & Rissman, 2017). The last denoising step was implemented in order to isolate movie-related
801 functional coupling from mere co-activation effects corresponding to the beginning and end of a
802 movie clip (i.e., two regions that are both activated at the beginning of a movie clip and de-
803 activated at its end, although they do not "communicate" with one another throughout the movie
804 clip). The residual BOLD time series were bandpass filtered ($0.008\ Hz < f < 0.09\ Hz$), linearly
805 detrended and despiked (all three are default CONN denoising steps). Following these
806 corrections (which again did not include global signal regression), an inspection of each subject's
807 histogram of voxel-to-voxel connectivity values revealed a normal distribution, approximately

centered around zero, which would suggest reduced contamination from physiological and motion-related confounds (cf. Whietfield-Gabrieli & Castanon, 2012). Nonetheless, in supplementary analyses, accompanying all the brain-behavior tests, we confirmed that all the reported effects were not driven by individual differences in motion, as they remained unchanged after controlling for the average relative (i.e., volume-to-volume) displacement per participant, a widely used motion metric (Power et al., 2012, 2015; Satterthwaite et al., 2013).

fMRI data analysis.

ROI time series. We followed the same steps as in the Cam-Can data in order to extract the timeseries from 229 ROIs from the Power et al. (2011) atlas.

Functional connectivity analyses. Pairwise coupling among the 229 ROIs was estimated in CONN, separately for each of the 14 movies. Periods of rest between consecutive movie clips were eliminated from the analyses. As in the Cam-Can data, the pairwise correlations among all the ROIs were expressed as Fisher's z-scores, all of which (i.e., positive and negative alike) were subsequently used to compute the indices of interest for all connectivity analyses.

To characterize individual differences in dynamic network structure, we broke down each movie clip into partially overlapping 40 s long windows for a total of 1152 windows. Similar to the Cam-Can analyses, pairwise coupling among the 229 ROIs was estimated in CONN using a sliding window of 40 s in length (40 volumes) with a two-TR gap in-between windows and a "hanning weighting" (i.e., greater weight to the scans in the middle of the window relative to the ones at the periphery) applied to all the time points within a window.

Network-level analyses. We followed the same steps as in the Cam-Can data with the following exceptions. We only computed similarity in functional brain organization (i.e., community structure) between consecutive windows, since, due to the shorter duration and the

structure of the HCP movie clips, narrative event boundaries were less legible and, as such, did not constitute a point of inquiry. Instead, to index brain sensitivity to object- versus action-related changes, we computed the Spearman's rank correlation between window-to-window similarity in functional brain organisation (i.e., community structure) and window-to-window noun- versus verb-based semantic similarity. Because we were specifically interested in brain-(noun/verb-based) movie *coupling*, overall window-to-window brain reconfiguration was regressed out from both indices. The two residual brain-movie (noun- vs. verb-based) couplings were used in all the reported analyses. Participation coefficients for each of the 229 ROIs were computed as in the Cam-Can dataset.

Reliability analyses. To test whether a unitary construct can be extracted for each neural index of interest across all 14 movies, we conducted separate reliability analyses on the 42 values associated with each index (i.e., three values for each of the 14 movies, corresponding to the community detection estimates obtained with a spatial resolution parameter of .95, 1, 1.05). Since subject motion can impact such reliability estimates, we present the relevant Cronbach's alpha values, both before and after regressing out subject level average frame-to-frame displacement (see Preprocessing above for the additional motion effect removal procedures already implemented). Additionally, to reflect the variables used in our analyses, for the brain-(noun/verb-based) movie coupling, we present reliability estimates based on data from which we regressed out both subject motion and spontaneous window-to-window functional brain reconfiguration.

For the window-to-window brain organisation similarity index, we obtained Cronbach's alphas of .87 and of .89 (with regression of the motion summary statistic). The brain-(noun) movie coupling index showed Cronbach's alphas of .66 and of .68 (with regression of motion

and window-to-window brain reconfiguration). For the brain-(verb) movie coupling index, we observed Cronbach's alphas of .65 and of .62 (with regression of motion and window-to-window brain reconfiguration). Across all 229 ROIs, the participation coefficients showed Cronbach's alphas between .76 and .98 (both with and without regression of the summary motion statistic).

Brain-behavior analyses

Canonical correlation analysis (CCA). We used canonical correlation analysis (CCA, Hotelling, 1936) with cross-validation procedures (cf. Hair et al., 2008) in order to characterize the relationships between our neural indices of interest (coupling between movie features and functional brain reorganization; ROI-specific diversity in functional interactions), as well as between the relevant brain (coupling between window-to-window changes in movie features and functional brain reorganization [dissimilarity in community structure]) and behavioral (fluid IQ, subclinical depression, subclinical anxiety) variables. Age was introduced in the CCAs in order to probe potential developmentally specific effects (Ofen et al., 2012; Petrican & Grady, 2017). As recommended in the literature (Hair et al., 1998), all CCAs were based on sample sizes more than ten times the number of variables in the analysis (Hair, Anderson, Tatham, & Black, 1998).

As in the Cam-Can data, the performance of our CCA-derived models was tested by using a 10-fold cross validation procedure. Specifically, the data were broken down into ten folds, six of which contained 18 participants (the remaining folds contained 17 participants each). The cross-validation procedure and relevant model descriptors were identical to those in the Cam-Can data. In both sets of CCAs, when evaluating the relationship between the predicted values of the two variates or the relationship between the actual value of each variable and the predicted value of its corresponding variate, we controlled for gender, handedness, subject-specific motion, years of education. In CCA 1 (see Figure 9) we additionally controlled for

877 current negative emotional experience to ensure that the observed associations are not due to

878 global negative mood around the time of testing.

879

880 **Materials & Correspondence.** Correspondence and material requests should be addressed to

881 R.P. (petricanr@cardiff.ac.uk).

882 **Data statement.** The raw data are available from https://camcan-archive.mrc-

883 cbu.cam.ac.uk/dataaccess/ (Cam-Can) and

884 https://db.humanconnectome.org/app/template/Login.vm;jsessionid=90091F006B15D5FA1D1D

885 9C3ED2D465DD (HCP) upon completion of the relevant data use agreements.

886 **Code availability.** We used already existing code, as specified in the main text.

References

Alderson, T., Bokde, A. L. W., Kelso, J. A. S., Maguire, L. & Coyle, D. (2020) Metastable neural dynamics underlies cognitive performance across multiple behavioural paradigms. *Human Brain Mapping, 41*, 3212-3234.

Andrews-Hanna, J.R., Smallwood, J.S., & Spreng, R.N. (2014). The default network and self-generated thought: Component processes, dynamic control, and clinical relevance. *Annals of New York Academy of Sciences - Year in Cognitive Neuroscience Special Issue, 1316*, 29-52.

Baldwin, D.A. & Kosie, J.E. (2020). How Does the Mind Render Streaming Experience as Events?. *Topics in Cognitive Sciences*. doi:10.1111/tops.12502

Barbey, A.K. (2018). Network neuroscience theory of human intelligence. *Trends in Cognitive Sciences*, *22*, 8-20.

Barch, D.M., Burgess, G.C., Harms, M.P., Petersen, S.E., Schlaggar, B.L., Corbetta, M., Glasser, M.F., Curtiss, S., Dixit, S., Feldt, C., Nolan, D., Bryant, E., Hartley, T., Footer, O., Bjork, J.M., Poldrack. R., Smith, S., Johansen-Berg, H., Snyder, A.Z., & Van Essen DC; for the WU-Minn HCP Consortium (2013). Function in the human connectome: Task-fMRI and individual differences in behavior. *NeuroImage, 80*, 169-189.

Bassett, D.S., Wymbs, N.F., Rombach, M.P., Porter, M.A., Mucha, P.J., & Grafton, S.T. (2013). Task-based core-periphery organisation of human brain dynamics. *PLoS Computational Biology, 9*, e1003171.

Bassett, D. S., Wymbs, N. F., Porter, M. A., Mucha, P. J., Carlson, J. M., & Grafton, S. T. (2011). Dynamic reconfiguration of human brain networks during learning. *Proceedings of the National Academy of Sciences of the United States of America, 108*, 7641-7646.

910 Belayachi, S. & Van der Linden, M. (2015) Exploring the parsing of dynamic action in checking
911 proneness. *Behaviour Change, 32,* 93-103.
912 Belzung, C., Wilner, P., & Philippot, P. (2015) Depression: from psychopathology to
913 pathophysiology. *Current Opinion in Neurobiology, 30,* 24-30.
914 Betzel, R. F., & Bassett, D. S. (2017). Multi-scale brain networks. *NeuroImage, 160*, 73-83.
915 Betzel, R. F., Byrge, L., He, Y., Goñi, J., Zuo, X., & Sporns, O. (2014). Changes in structural
916 and functional connectivity among resting-state networks across the human
917 lifespan. *NeuroImage, 102*, 345-357.
918 Betzel, R. F., Fukushima, M., He, Y., Zuo, X., & Sporns, O. (2016). Dynamic fluctuations
919 coincide with periods of high and low modularity in resting-state functional brain
920 networks. *NeuroImage, 127*, 287-297.
921 Bolt, T., Nomi, J. S., Rubinov, M., & Uddin, L. Q. (2017). Correspondence between evoked and
922 intrinsic functional brain network configurations. *Human Brain Mapping, 38*, 1992-
923 2007.
924 Bonnici, H.M., Richter, F.R., Yazar, Y., & Simons, J.S. (2016). Multimodal feature integration
925 in the angular gyrus during episodic and semantic retrieval. *Journal of Neuroscience, 36*,
926 5462–71.
927 Branzi, F.M., Humphreys, G.F., Hoffman, P., & Lambon Ralph, M.A. (2020) Revealing the
928 neural networks that extract conceptual gestalts from continuously evolving or changing
929 semantic contexts. *NeuroImage*. https://doi.org/10.1016/j.neuroimage.2020.116802.
930 Braun, U., Schäfer, A., Walter, H., Erk, S., Romanczuk-Seiferth, N., Haddad, L., . . . Bassett, D.
931 S. (2015). Dynamic reconfiguration of frontal brain networks during executive cognition

in humans. *PNAS Proceedings of the National Academy of Sciences of the United States of America, 112*, 11678-11683.

Brewin, C. R., Gregory, J. D., Lipton, M., & Burgess, N. (2010). Intrusive images in psychological disorders: Characteristics, neural mechanisms, and treatment implications. *Psychological Review, 117*, 210–232.

Buckner, R. L., Krienen, F. M., Castellanos, A., Diaz, J. C., & Yeo, B. T. T. (2011). The organization of the human cerebellum estimated by intrinsic functional connectivity. *Journal of Neurophysiology, 106*, 2322-2345.

Cao, H., Plichta, M. M., Schäfer, A., Haddad, L., Grimm, O., Schneider, M., . . . Tost, H. (2014). Test–retest reliability of fMRI-based graph theoretical properties during working memory, emotion processing, and resting state. *NeuroImage, 84*, 888-900.

Cattell, R.B. (1971) *Abilities: Their structure, growth, and action*. Boston: Houghton Mifflin.

Cattell, R.B. & Cattell, H.E.P. (1973) *Measuring intelligence with the culture fair tests*. Champaign, IL: The Institute for Personality and Ability Testing.

Chan, M., Park, D.C., Savalia, N.K., Petersen, S.E., & Wig, G.S. (2014). Decreased segregation of brain systems across the healthy adult lifespan. *Proceedings of the National Academy of Sciences of the United States of America, 111*, E4997–E5006.

Chang, C. & Glover, G.H. (2010). Time-frequency dynamics of resting state brain connectivity measured with fMRI. *NeuroImage 50*, 81–98.

Chen, J., Leong, Y.C., Honey, C.J., Yong, C.H., Norman, K.A., & Hasson, U. (2017). Shared memories reveal shared structure in neural activity across individuals. *Nature Neuroscience, 20*, 115-130.

954 Chen, J., Honey, C.J., Simony, E., Arcaro, M.J., Norman, K.A., & Hasson, U. (2016). Accessing
955 real-life episodic information from minutes versus hours earlier modulates hippocampal
956 and high-order cortical dynamics. *Cerebral Cortex, 26,* 3428-3441.
957 Chen, T., Cai, W., Ryali, S., Supekar, K., & Menon, V. (2016). Distinct global brain dynamics
958 and spatiotemporal organization of the salience network. *PLoS Biology, 14*, 21.
959 Chiou, R., Humphreys, G. F, & Lambon Ralph, M. A. (2020) Bipartite functional fractionation
960 within the default network supports disparate forms of internally oriented cognition,
961 *Cerebral Cortex*. DOI: 10.1093/cercor/bhaa130
962 Cicchetti, D. V., & Sparrow, S. A. (1981). Developing criteria for establishing interrater
963 reliability of specific items: Applications to assessment of adaptive behavior. *American*
964 *Journal of Mental Deficiency, 86*, 127-137.
965 Colzato L.S., Wouwe N.C. van, Lavender T. & Hommel B. (2006), Intelligence and cognitive
966 flexibility: Fluid intelligence correlates with feature "unbinding" across perception and
967 action. *Psychonomic Bulletin & Review, 13*, 1043-1048.
968 Corbetta, M., Kincade, J. M., Ollinger, J. M., McAvoy, M. P., & Shulman, G. L. (2000).
969 Voluntary orienting is dissociated from target detection in human posterior parietal
970 cortex. *Nature Neuroscience, 3*, 292-297.
971 Corbetta, M. & Shulman, G.L. (2002). Control of goal-directed and stimulus-driven attention in
972 the brain. *Nature Reviews Neuroscience, 3*, 201–215.
973 Crawford, J.D. & Stankov, L. (1996). Age differences in the realism of confidence judgements:
974 A calibration study using tests of fluid and crystallized intelligence. *Learning and*
975 *Individual Differences, 8,* 83-103.

976 Cutting, J.E., Brunick, K.L., & Candan, A. (2012). Perceiving event dynamics and parsing
977 Hollywood films. *Journal of Experimental Psychology: Human Perception and*
978 *Performance, 38*, 1476-90.
979 D'Argembeau, A., & Van, d. L. (2006). Individual differences in the phenomenology of mental
980 time travel: The effect of vivid visual imagery and emotion regulation
981 strategies. *Consciousness and Cognition: An International Journal, 15*, 342-350.
982 Daselaar, S. M., Rice, H. J., Greenberg, D. L., Cabeza, R., LaBar, K. S., & Rubin, D. C. (2008).
983 The spatiotemporal dynamics of autobiographical memory: Neural correlates of recall,
984 emotional intensity, and reliving. *Cerebral Cortex, 18*, 217-229.
985 Dixon, M. L., De la Vega, A., Mills, C., Andrews-Hanna, J., Spreng, R., Cole, M. W., Christoff,
986 K. (2018) Heterogeneity within the frontoparietal control network and its relationship to
987 the default and dorsal attention networks. *Proceedings of the National Academy of*
988 *Sciences of the United States of America, 115,* E1598–E1607.
989 Duncan, J., Assem, M., & Shashidhara, S. (2020) Integrated intelligence from distributed brain
990 activity. *Trends in Cognitive Sciences.* https://doi.org/10.1016/j.tics.2020.06.012
991 Duncan, J., Chylinski, D., Mitchell, D.J., & Bhandari, A. (2017) Fluid intelligence and cognitive
992 segmentation. *Proceedings of the National Academy of Sciences of the United States of*
993 *America, 114,* 5295-5299.
994 Finc, K., Bonna, K., He, X., Lydon-Staley, D.M., Kuhn, S., Duch, W., & Bassett, D.S. (2020)
995 Dynamic reconfiguration of functional brain networks during working memory training.
996 *Nature Communications, 11*, 2435.
997 Fornito, A., Zalesky, A., & Bullmore, E. T. (2016). Fundamentals of Brain Network Analysis. (1
998 ed.) Academic Press.

Fox, M. D., & Raichle, M. E. (2007). Spontaneous fluctuations in brain activity observed with functional magnetic resonance imaging. *Nature Reviews Neuroscience, 8*, 700–711.

Fox, M. D., Snyder, A. Z., Vincent, J. L., Corbetta, M., Van Essen, D. C., & Raichle, M. E. (2005). The human brain is intrinsically organized into dynamic, anticorrelated functional networks. *Proceedings of the National Academy of Sciences of the United States of America, 102*, 9673-9678.

Freton, M., Lemogne, C., Bergouignan, L., Delaveau, P., Lehéricy, S., & Fossati, P. (2014). The eye of the self: Precuneus volume and visual perspective during autobiographical memory retrieval. *Brain Structure & Function, 219*, 959-968.

Garrett, D.D., Epp, S.M., Kleemeyer, M., Lindenberger, U., and Polk, T.A. (2020). Higher performing older adults upregulate brain signal variability in response to feature-rich sensory input. *NeuroImage, 217*, 116836.

Garrett, D.D., Nagel, I.E., Preuschhof, C., Burzynska, A.Z., Marchner, J., Wiegert, S., Jungehülsing, G., Nyberg, L., Villringer, A., Li, S-C., Heekeren, H.E., Bäckman, L., & Lindenberger, U. (2015). Amphetamine modulates brain signal variability and working memory in younger and older adults. *Proceedings of the National Academy of Sciences of the United States of America, 112*, 7593-7598.

Geerligs, L., Cam-CAN, & Campbell, K.L. (2018) Age-related differences in information processing during movie watching. *Neurobiology of Aging, 72*, 106-120.

Gilson, M., Deco, G., Friston, K.J., Hagmann, P., Mantini, D., Betti, V., Romani, G.L., & Corbetta, M. (2018) Effective connectivity inferred from fMRI transition dynamics during movie viewing points to a balanced reconfiguration of cortical interactions. *NeuroImage, 180*, 534-546.

1022 Gonzalez-Castillo, J. & Bandettini, P. A. (2018) Task-based dynamic functional connectivity:
1023 Recent findings and open questions. *NeuroImage, 180,* 526-533.
1024 Grady, C.L. & Garrett, D.D. (2018). Brain Signal Variability is Modulated as a Function of
1025 Internal and External Demand in Younger and Older Adults. *NeuroImage, 169*, 510-523.
1026 Gur, R.C., Ragland, J.D., Moberg, P.J., Bilker, W.B., Kohler, C., Siegel, S.J., Gur, R.E. (2001a).
1027 Computerized neurocognitive scanning: II. The profile of schizophrenia.
1028 *Neuropsychopharmacology, 25*, 777–788.
1029 Gur, R.C., Ragland, J.D., Moberg, P.J., Turner, T.H., Bilker, W.B., Kohler, C., Siegel, S.J., &
1030 Gur, R.E. (2001b). Computerized neurocognitive scanning: I. Methodology and
1031 validationin healthy people. *Neuropsychopharmacology, 25,* 766–776.
1032 Gur, R.C., Richard, J., Hughett, P., Calkins, M.E., Macy, L., Bilker, W.B., Brensinger, C., &
1033 Gur, R.E. (2010). A cognitive neuroscience-based computerized battery for efficient
1034 measurement of individual differences: standardization and initial construct validation.
1035 *Journal of Neuroscience Methods, 187*, 254–262.
1036 Hasson, U., Chen, J., & Honey, C.J. (2015). Hierarchical process memory: memory as an
1037 integral component of information processing. *Trends in Cognitive Sciences, 19*, 304-
1038 313.
1039 Hermans, E.J., Henckens, M.J.A.G., Joëls, M., Fernández, G. (2014). Dynamic adaptation of
1040 large-scale brain networks in response to acute stressors. *Trends in Neurosciences, 37*,
1041 304–314.
1042 Hilger, K., Fukushima, M., Sporns, O., & Fiebach, C.J. (2019) Temporal stability of functional
1043 brain modules associated with human intelligence. *Human Brain Mapping, 41,* 362-372.

1044 Hitchcock, A. (1961). Bang! You're Dead Los Angeles: National Broadcasting Company
1045 (NBC).
1046 Hoffman, P., McClelland, J.L., Lambon Ralph, M.A. (2018). Concepts, control, and context: A
1047 connectionist account of normal and disordered semantic cognition. *Psychological*
1048 *Review, 125*, 293-328.
1049 Honey, C.J., Newman, E.L., & Schapiro, A.C. (2017). Switching between internal and external
1050 modes: a multi-scale learning principle. *Network Neuroscience, 1*, 339–356.
1051 Humphreys, G.F. & Lambon Ralph, M.A. (2015). Fusion and Fission of Cognitive Functions in
1052 the Human Parietal Cortex. *Cerebral Cortex, 25*, 3547-3560.
1053 Iraji, A., Faghiri, A., Lewis, N., Fu, Z., Rachakonda, S. & Calhoun, V.D. (2020) Tools of the
1054 trade: Estimating time-varying connectivity patterns from fMRI data. *Social Cognitive*
1055 *and Affective Neuroscience, nsaa114*. https://doi.org/10.1093/scan/nsaa114
1056 Irish, M., Halena, S., Kamminga, J., Tu, S., Hornberger, M., Hodges, J. (2015). Scene
1057 construction impairments in Alzheimer's disease: A unique role for the posterior
1058 cingulate cortex. *Cortex, 73*, 10-23.
1059 Hair, J.F., Tatham, R.L., Anderson, R.E . & Black, W, (1998) Multivariate data analysis. (Fifth
1060 Ed.) Prentice-Hall: London.
1061 Hair Jr., J.F., Black, W.C., Babin, B.J. & Anderson, R.E. (2009) Multivariate Data Analysis.
1062 (Seventh Ed.) Prentice Hall: Upper Saddle River, 761.
1063 Hasson, U., Landesman, O., Knappmeyer, B., Vallines, I., Rubin, N., & Heeger, D.J. (2008)
1064 Neurocinematics: The neuroscience of film. *Projections, 2*, 1–26.
1065 Hasson, U., Malach, R., & Heeger, D.J. (2010) Reliability of cortical activity during natural
1066 stimulation. *Trends in Cognitive Sciences, 14*, 40–48.

1067 Hebscher, M., Levine, B., & Gilboa, A. (2018). The precuneus and hippocampus contribute to
1068 individual differences in the unfolding of spatial representations during episodic
1069 autobiographical memory. *Neuropsychologia, 110*, 123-133.
1070 Hutchison, R.M. & Morton, J.B. (2015) Tracking the brain's functional coupling dynamics over
1071 development. *Journal of Neuroscience*, *35*, 6849–6859.
1072 Hutchison, R.M., Womelsdorf, T., Gati, J.S., Everling, S., & Menon, R.S. (2013). Resting-state
1073 networks show dynamic functional connectivity in awake humans and anesthetized
1074 macaques. *Human Brain Mapping, 34*, 2154–2177.
1075
1076 Huth, A.G., Nishimoto, S., Vu, A., & Gallant, J.L. (2012). A continuous semantic space
1077 describes the representation of thousands of object and action categories across the
1078 human brain. *Neuron*, 76, 1210-1224.
1079 Kao, C.-H., Khambhati, A.N., Bassett, D.S., Nassar, M.R., McGuire, J.T., Gold, J.I., & Kable,
1080 J.W. (2020). Functional brain network reconfiguration during learning in a dynamic
1081 environment. *Nature Communications, 11*, 1682.
1082 Kashtan, N. & Alon, U. (2005) Spontaneous evolution of modularity and network motifs.
1083 *Proceedings of the National Academy of Sciences, 102*, 13773–13778.
1084 Kashtan, N., Noor, E., & Alon, U. (2007) Varying environments can speed up evolution.
1085 *Proceedings of the National Academy of Sciences, 104*, 13711–13716.
1086 Kettinger, A., Hill, C., Vidnyánszky, Z., Windischberger, C., & Nagy, Z. (2016). Investigating
1087 the Group-Level Impact of Advanced Dual-Echo fMRI Combinations. *Frontiers in*
1088 *Neuroscience*, 10: 571.
1089 Kurby, C. A., & Zacks, J. M. (2018). Preserved neural event segmentation in healthy older
1090 adults. *Psychology and Aging, 33*, 232.

Kurby, C.A. & Zacks, J.M. (2011). Age differences in the perception of hierarchical structure in events. *Memory & Cognition, 39*, 75–91.

Lancichinetti, A. & Fortunato, S. (2009) Community detection algorithms: A comparative analysis. *Physical Review E, 80*, 056117.

Laumann, T. O., Snyder, A. Z., Mitra, A., Gordon, E. M., Gratton, C., Adeyemo, B., . . . Petersen, S. E. (2017). On the stability of BOLD fMRI correlations. *Cerebral Cortex, 27*, 4719-4732.

Lenhard, W. & Lenhard, A. (2014). Hypothesis Tests for Comparing Correlations. available: https://www.psychometrica.de/correlation.html. Bibergau (Germany): Psychometrica. DOI: 10.13140/RG.2.1.2954.1367

Leonardi, N., & Ville, V. D. (2015). On spurious and real fluctuations of dynamic functional connectivity during rest. *NeuroImage, 104*, 430-436.

Levine, D., Buchsbaum, D., Hirsh-Pasek, K., & Golinkoff, R. M. (2019). Finding events in a continuous world: A developmental account. *Developmental Psychobiology, 61*, 376-389.

Lurie, D.J., Kessler, D., Bassett, D.S., Betzel, R.F., Breakspear, M., Kheilholz, S.…& Calhoun, V.D. (2020). Questions and controversies in the study of time-varying functional connectivity in resting fMRI. *Network Neuroscience, 4*, 30-69.

Magliano, J.P. & Zacks, J. M. (2011). The impact of continuity editing in narrative film on event segmentation. *Cognitive Sciences, 35,* 1489–1517.

Marusak, H. A., Calhoun, V. D., Brown, S., Crespo, L. M., Sala-Hamrick, K., Gotlib, I. H., & Thomason, M. E. (2017). Dynamic functional connectivity of neurocognitive networks in children. *Human Brain Mapping, 38*, 97-108.

1113 Mathews, A. Yiend, J. & Lawrence, A.D. (2004) Individual Differences in the Modulation of
1114 Fear-Related Brain Activation by Attentional Control. *Journal of Cognitive*
1115 *Neuroscience, 16*, 1683-1694.
1116 Mesulam, M.M. (1998) From sensation to cognition. *Brain, 121*, 1013–1052.
1117 Murphy, K. & Fox, M.D. (2017) Towards a consensus regarding global signal regression for
1118 resting state functional connectivity MRI. *NeuroImage, 154*, 169-173.
1119 Ofen, N., Chai, X.J., Schuil, K.D., Whitfield-Gabrieli, S., & Gabrieli, J.D. (2012) The
1120 development of brain systems associated with successful memory retrieval of scenes.
1121 *Journal of Neuroscience, 32*, 10012–10020.
1122 Padmanabhan, K. & Urban, N.N. (2010). Intrinsic biophysical diversity decorrelates neuronal
1123 firing while increasing information content. *Nature Neuroscience, 13*, 1276–1282.
1124 Petrican, R. & Grady, C.L. (2017). Contextual and developmental differences in the neural
1125 architecture of cognitive control. *Journal of Neuroscience, 37,* 7711-7726.
1126 Petrican, R., Saverino, C., Rosenbaum, R.S. and Grady, C. (2015). Inter-individual differences in
1127 the experience of negative emotion predict variations in functional brain architecture.
1128 *NeuroImage, 123*, 80-88.
1129 Poldrack, R. & Shine, J.M. (2018) Principles of dynamic network reconfiguration across diverse
1130 brain states. *NeuroImage, 180,* 396-405.
1131 Poser, B.A., Versluis, M. J., Hoogduin, J. M., & Norris, D. G. (2006). BOLD contrast sensitivity
1132 enhancement and artifact reduction with multiecho EPI: Parallel-acquired
1133 inhomogeneity-desensitized fMRI. *Magnetic Resonance in Medicine, 55*, 1227–1235.
1134 Power, J.D., Cohen, A.L., Nelson, S.M., Wig, G.S., Barnes, K.A., ...& Petersen, S. E. (2011)
1135 Functional network organization of the human brain. *Neuron, 72*, 665–678.

1136 Power, J.D., Barnes, K.A., Snyder, A.Z., Schlaggar, B.L., & Petersen, S.E. (2012). Spurious but
1137 systematic correlations in functional connectivity MRI networks arise from subject
1138 motion. *NeuroImage, 59*, 2142-2154.
1139 Power, J. D., Schlaggar, B. L., & Petersen, S. E. (2015). Recent progress and outstanding issues
1140 in motion correction in resting state fMRI. *NeuroImage, 105*, 536-551.
1141 Preti, M. G., Bolton, T. A. W., & Ville, V. D. (2017). The dynamic functional connectome:
1142 State-of-the-art and perspectives. *NeuroImage, 160*, 41-54.
1143 Radvansky, G. A. & Dijkstra, K. (2007). Aging and situation model processing. *Psychonomic*
1144 *Bulletin Review, 14*, 1027–42
1145 Radvansky, G. A., & Zacks, J. M. (2017). Event boundaries in memory and cognition. *Current*
1146 *Opinion in Behavioral Sciences, 17*, 133-140.
1147 Ramanan, S., Piguet, O., Irish, M. (2018). Rethinking the role of the angular gyrus in
1148 remembering the past and imagining the future: The Contextual Integration Model. *The*
1149 *Neuroscientist, 24*, 342-352.
1150 Ranganath, C. & Ritchey, M. (2012). Two cortical systems for memory-guided behaviour.
1151 *Nature Reviews Neuroscience, 13*, 713-726.
1152 Reagh, Z.M., Delarazan, A.I., Garber, A., & Ranganath, C. (2020). Aging alters neural activity at
1153 event boundaries in the hippocampus and Posterior Medial network. *Nature*
1154 *Communications, 11,* 3980.
1155 Richter, F.R., Cooper, R.A., Bays, P.M., & Simons, J.S. (2016). Distinct neural mechanisms
1156 underlie the success, precision, and vividness of episodic memory. *Elife*, 5.

1157 Rissman, J., Chow, T.E., Reggente, N., Wagner, A.D. (2016). Decoding fMRI signatures of real-
1158 world autobiographical memory retrieval. *Journal of Cognitive Neuroscience, 28*, 604–
1159 20.
1160 Ritchey, M. & Cooper, R. (2020) Deconstructing the Posterior Medial Episodic Network. *Trends*
1161 *in Cognitive Sciences, 24*, 451 – 465.
1162 Rosvall, M. & Bergstrom, C.T. (2008). Maps of random walks on complex networks reveal
1163 community structure. *Proceedings of the National Academy of Sciences of the United*
1164 *States of America, 105*, 1118-1123.
1165 Rubinov, M. & Sporns O. (2010) Complex network measures of brain connectivity: uses and
1166 interpretations. *NeuroImage, 52*,1059–1069.
1167 Rubinov, M. & Sporns O. (2011) Weight-conserving characterization of complex functional
1168 brain networks. *NeuroImage, 56*,2068-2079.
1169 Rugg, M.D. & Vilberg, K.L. (2013). Brain networks underlying episodic memory retrieval.
1170 *Current Opinion in Neurobiology, 23*, 255–60.
1171 Sadaghiani, S. & D'Esposito, M. (2015) Functional characterization of the cingulo-opercular
1172 network in the maintenance of tonic alertness. *Cerebral Cortex, 25*, 2763–2773.
1173 Sargent, J. Q., Zacks, J. M., Hambrick, D. Z., Zacks, R. T., Kurby, C. A., Bailey, H. R., . . .
1174 Beck, T. M. (2013). Event segmentation ability uniquely predicts event memory.
1175 *Cognition, 129*, 241–255.
1176 Satterthwaite, T.D., Wolf, D.H., Ruparel, K., Erus, G., Elliott, M.A., Eickhoff, S.B., Gennatas,
1177 E.D., Jackson, C., Prabhakaran, K.,Smith, A., Hakonarson, H., Verma, R., Davatzikos,
1178 C., Gur, R.E., & Gur, R.C. (2013). Heterogeneous impact of motion on fundamental

patterns of developmental changes in functional connectivity during youth. *NeuroImage, 83,* 45–57.

Satterthwaite, T. D., Wolf, D. H., Roalf, D. R., Ruparel, K., Erus, G., Vandekar, S., . . . & Gur, R. C. (2015). Linked sex differences in cognition and functional connectivity in youth. *Cerebral Cortex, 25*(9), 2383-2394.

Schultz, D. H., & Cole, M. W. (2016). Higher intelligence is associated with less task-related brain network reconfiguration. *The Journal of Neuroscience, 36*, 8551-8561.

Shafto, M.A., Tyler, L.K., Dixon, M., Taylor, J.R., Rowe, J.B., Cusack, R., Calder, A.J., Marslen-Wilson, W.D., Duncan, J., Dalgleish, T., Henson, R.N., Brayne, C., Matthews, F.E.; Cam-CAN (2014) The Cambridge Centre for Ageing and Neuroscience (Cam-CAN) study protocol: a cross-sectional, lifespan, multidisciplinary examination of healthy cognitive ageing. *BMC Neurology, 14*, 204.

Sherrill, A.M., Kurby, C.A., Lilly, M.M. & Magliano, J.P. (2019) The effects of state anxiety on analogue peritraumatic encoding and event memory: Introducing the stressful event segmentation paradigm, *Memory, 27*, 124-136,

Sherry, A., & Henson, R. K. (2005). Conducting and interpreting canonical correlation analysis in personality research: A user-friendly primer. *Journal of Personality Assessment, 84*, 37-48.

Smith, S. M., M. Jenkinson, M.W. Woolrich, C.F. Beckmann, T.E.J. Behrens, … & P.M. Matthews (2004). Advances in functional and structural MR image analysis and implementation as FSL. *NeuroImage, 23*, 208-219.

1200 Smith, S.M., Beckmann, C.F., Andersson, J., Auerbach, E.J., Bijsterbosch, J., Douaud, G., et al.
1201 (2013). Resting-state fMRI in the Human Connectome Project. *NeuroImage, 80,* 144–
1202 168.
1203 Smith, S. M., Nichols, T. E., Vidaurre, D., Winkler, A. M., Behrens, T. E. J., Glasser, M. F., . . .
1204 Miller, K. L. (2015). A positive-negative mode of population covariation links brain
1205 connectivity, demographics and behavior. *Nature Neuroscience, 18*, 1565-1567.
1206 Sporns, O. & Betzel, R.F. (2016). Modular brain networks. *Annual Review of Psychology, 67*,
1207 613-640.
1208 Spreng, R.N., Stevens, W.D., Chamberlain, J.P., Gilmore, A.W., Schacter, D.L., 2010. Default
1209 network activity, coupled with the frontoparietal control network, supports goal-directed
1210 cognition. *NeuroImage, 53*, 303–317.
1211 Spreng, R.N. & Turner, G.R. (2019) The shifting architecture of cognition and brain function in
1212 older adulthood. *Perspectives on Psychological Science, 14*, 523 –542.
1213 Stawarcyzk, D., Bezdek, M. A., & Zacks, J. M. (2019). Event representations and predictive
1214 processing: The role of the midline default network core. *Topics in Cognitive Science*, 1-
1215 23.
1216 Swallow, K.M., Kemp, J.T., & Simsek, A.C. (2018) The role of perspective in event
1217 segmentation. *Cognition, 177*, 249-262.
1218 Sylvester, C.M., Corbetta, M., Raichle, M.E., Rodebaugh, T.L., Schlaggar, B.L., Sheline, Y.I.,
1219 Zorumski, C.F., & Lenze, E.J. (2012) Functional network dysfunction in anxiety and
1220 anxiety disorders. *Trends in Neurosciences, 35*, 527-535.
1221 Taylor, J.R., Williams, N., Cusack, R., Auer, T., Shafto, M.A., Dixon, M., Tyler, L.K., Cam-
1222 CAN, Henson, R.N. (2017). The Cambridge Centre for Ageing and Neuroscience (Cam-

CAN) data repository: Structural and functional MRI, MEG, and cognitive data from a cross-sectional adult lifespan sample. *NeuroImage, 144*, 262-269.

Telesford, Q. K., Lynall, M., Vettel, J., Miller, M. B., Grafton, S. T., & Bassett, D. S. (2016). Detection of functional brain network reconfiguration during task-driven cognitive states. *NeuroImage, 142*, 198-210.

Thakral, P.P., Madore, K.P., & Schacter, D.L. (2017). A role for the left angular gyrus in episodic simulation and memory. *Journal of Neuroscience, 37*, 8142–9.

Thompson, W.H., Kastrati, G., Finc, K., Wright, J., Shine, J.M., & Poldrack, R.A. (2020) Time-varying nodal measures with temporal community structure: A cautionary note to avoid misinterpretation. *Human Brain Mapping, 41*, 2347-2356. doi: 10.1002/hbm.24950.

Tsvetanov, K. A., Henson, R. N. A., Tyler, L. K., Razi, A., Geerligs, L., Ham, T. E., & Rowe, J. B. (2016). Extrinsic and intrinsic brain network connectivity maintains cognition across the lifespan despite accelerated decay of regional brain activation. *The Journal of Neuroscience, 36*, 3115-3126.

Tulving, E. (2002) Episodic memory: From mind to brain. *Annual Review of Psychology, 53,* 1-25.

Tulving, E. (1985). Memory and consciousness. *Canadian Psychology/Psychologie Canadienne, 26*, 1-12.

Turner, G. R., & Spreng, R. N. (2015). Prefrontal engagement and reduced default network suppression co-occur and are dynamically coupled in older adults: The default-executive coupling hypothesis of aging. *Journal of Cognitive Neuroscience, 27*, 2462–2476.

Umanath, S., & Marsh, E. J. (2014). Understanding how prior knowledge influences memory in older adults. *Perspectives on Psychological Science, 9*, 408–426.

1246 Uncapher, M.R. & Rugg, M.D. (2009). Selecting for Memory? The Influence of Selective
1247 Attention on the Mnemonic Binding of Contextual Information. *Journal of Neuroscience,*
1248 *29,* 8270-8279.
1249 Vanderwal, T., Eilbott, J. Finn, E.S., Craddock, R.C., Turnbull, A. & Castellanos, F.X. (2017)
1250 Individual differences in functional connectivity during naturalistic viewing conditions.
1251 *NeuroImage, 157*, 521-530.
1252 Vannucci, M., Pelagatti, C., Chiorri, C., & Mazzoni, G. (2016). Visual object imagery and
1253 autobiographical memory: Object imagers are better at remembering their personal
1254 past. *Memory, 24*, 455-470.
1255 Vatansever, D., Menon, D. K., Manktelow, A. E., Sahakian, B. J., & Stamatakis, E. A. (2015).
1256 Default mode dynamics for global functional integration. *The Journal of*
1257 *Neuroscience, 35*, 15254-15262.
1258 Vatansever, D., Bzdok, D., Wang, H., Mollo, G., Sormaz, M., Murphy, C., . . . Jefferies, E.
1259 (2017). Varieties of semantic cognition revealed through simultaneous decomposition of
1260 intrinsic brain connectivity and behaviour. *NeuroImage, 158*, 1-11.
1261 Vatansever, D., Menon, D. K., & Stamatakis, E. A. (2017). Default mode contributions to
1262 automated information processing. *PNAS Proceedings of the National Academy of*
1263 *Sciences of the United States of America, 114*, 12821-12826.
1264 Vinh, N.X, Epps, J., & Bailey, J. (2010). Information theoretic measures for clusterings
1265 comparison: Variants, properties, normalization and correction for chance. *Journal of*
1266 *Machine Learning Research, 11*, 2837-2854.
1267 Wagner, A.D., Shannon, B.J., Kahn, I., & Buckner, R.L. (2005). Parietal lobe contributions to
1268 episodic memory retrieval. *Trends in Cognitive Sciences, 9*, 445–53.

1269 Wang, H.-T., Smallwood, J., Mourao-Miranda, J., Xia, C.H., Satterthwaite, T.D., Bassett, D.S.
1270 & Bzdok, D. Finding the needle in a high-dimensional haystack: Canonical correlation
1271 analysis for neuroscientists. NeuroImage, 216, 116745.
1272 Westphal, A. J., Reggente, N., Ito, K. L., & Rissman, J. (2016). Shared and distinct contributions
1273 of rostrolateral prefrontal cortex to analogical reasoning and episodic memory
1274 retrieval. *Human Brain Mapping, 37*, 896-912.
1275 Wheatley, T., Milleville, S.C., & Martin, A. (2007). Understanding animate agents: distinct roles
1276 for the social network and mirror system. *Psychological Science, 18*, 469–474.
1277 Wheeler, M. E., & Buckner, R. L. (2004). Functional-anatomic correlates of remembering and
1278 knowing. *NeuroImage, 21*, 1337–1349.
1279 Whitfield-Gabrieli, S. & Nieto-Castanon, A. (2012). CONN: a functional connectivity toolbox
1280 for correlated and anticorrelated brain networks. *Brain Connectivity, 2*, 125-141.
1281 Wig, G.S., Schlaggar, B.L.,Petersen,S.E. (2011). Concepts and principles in the analysis of brain
1282 networks. *Annals of the New York Academy of Sciences,1224*, 126–146.
1283 Xia, M., Wang, J., & He, Y. (2013) BrainNet Viewer: A Network Visualization Tool for Human
1284 Brain Connectomics. *PLoS ONE 8*: e68910.
1285 Yarkoni, T., Poldrack, R. A., Nichols, T. E., Van Essen, D. C., & Wager, T. D. (2011). Large-
1286 scale automated synthesis of human functional neuroimaging data. *Nature Methods, 8*,
1287 665–670.
1288 Yazar, Y., Bergstrom, Z.M., & Simons, J.S. (2017). Reduced multimodal integration of memory
1289 features following continuous theta burst stimulation of angular gyrus. *Brain Stimulation,*
1290 *10*, 624–9.

Yeo, B. T. T., Krienen, F. M., Sepulcre, J., Sabuncu, M. R., Lashkari, D., Hollinshead, M., . . . Buckner, R. L. (2011). The organization of the human cerebral cortex estimated by intrinsic functional connectivity. *Journal of Neurophysiology, 106*, 1125-1165.

Zacks, J. M. (2020). Event perception and memory. *Annual Review of Psychology, 71*, 165-191.

1297 Figure Captions

1298 Figure 1. *Schematic representation of the main preprocessing and analysis steps across both*
1299 *samples.*

1300 Figure 2. *Network structure in each of the seven age groups of the Cam-Can adult lifespan*
1301 *sample at 2-10% tie densities shows very similar levels of similarity to that of Power et al.'s*
1302 *(2011). The coloured lines show the normalized mutual information index (NMI),*
1303 *a highly used metric of similarity in community assignment, for each age group and tie density*
1304 *scrutinized.*

1305 Figure 3. *Age, intelligence and functional brain reconfiguration. The correlation coefficients*
1306 *(panels [a],[d]) and the standardized coefficients (panels [b],[e]) of the brain and behavioural*
1307 *variables on their corresponding canonical variate across all test CCAs, as well as the scatter*
1308 *plot describing the linear association between the two canonical variates across all the "test"*
1309 *folds (panel [c]). The scatter plot in panel (c) is based on standardized variables. In panels (a),*
1310 *(b),(d), and (e), white boxes correspond to coefficients that were not robust across all the*
1311 *bootstrapping samples, as described in the text. In all these analyses, gender, handedness, ROI*
1312 *homogeneity and the summary motion metric were introduced as covariates.*

1313 Figure 4. *Functional brain reconfiguration and network participation in older adulthood. The*
1314 *correlation coefficients (panels [a],[d]) and the standardized coefficients (panels [b],[e]) of the*
1315 *brain and behavioural variables on their corresponding canonical variate across all test CCAs,*
1316 *as well as the scatter plot describing the linear association between the two canonical variates*
1317 *across all the "test" folds (panel [c]). The scatter plot in panel (c) is based on standardized*
1318 *variables. In panels (a), (b),(d), and (e), white boxes correspond to coefficients that were not*
1319 *robust across all the bootstrapping samples, as described in the text. In all these analyses,*

gender, handedness, ROI homogeneity and the summary motion metric were introduced as covariates.

Figure 5. *Functional brain reconfiguration and network participation in younger adulthood. The correlation coefficients (panels [a],[d]) and the standardized coefficients (panels [b],[e]) of the brain and behavioural variables on their corresponding canonical variate across all test CCAs, as well as the scatter plot describing the linear association between the two canonical variates across all the "test" folds (panel [c]). The scatter plot in panel (c) is based on standardized variables. In panels (a), (b),(d), and (e), white boxes correspond to coefficients that were not robust across all the bootstrapping samples, as described in the text. In all these analyses, gender, handedness, ROI homogeneity and the summary motion metric were introduced as covariates.*

Figure 6. *Scatterplot describing the association between the fluid intelligence score and the network participation profile linked to functional reconfiguration in younger adulthood, after controlling for all the covariates described in the text.*

Figure 7. Panel (a). *Results of the PLS analysis, showing the ROIs that demonstrated robust associations with context-based functional brain reconfiguration across the lifespan. The brain regions were visualized with the BrainNet Viewer (http://www.nitrc.org/projects/bnv/) (Xia et al., 2013).* ROI colours reflect Power et al.'s network assignments (orange, DMN; pink, AUD). Panel (b) *Results of the Neurosynth decoding analysis based on the ROIs in panel (a).*

Figure 8. Panel (a). *Results of the PLS analysis, showing the ROIs that demonstrated robust associations with window-to-window functional brain reconfiguration across the lifespan. The brain regions were visualized with the BrainNet Viewer (http://www.nitrc.org/projects/bnv/) (Xia et al., 2013).* ROI colours reflect Power et al.'s network assignments (orange, DMN; blue, VIS;

yellow, FPC). Panel (b) *Results of the Neurosynth decoding analysis based on the ROIs in panel (a).*

Figure 9. *Brain-movie coupling and cognitive-affective function in the HCP sample. The correlation coefficients (panels [a],[d]) and the standardized coefficients (panels [b],[e]) of the brain and behavioural variables on their corresponding canonical variate across all test CCAs, as well as the scatter plot describing the linear association between the two canonical variates across all the "test" folds (panel [c]). The scatter plot in panel (c) is based on standardized variables. In panels (a), (b),(d), and (e), white boxes correspond to coefficients that were not robust across all the bootstrapping samples, as described in the text. In all these analyses, gender, handedness, years of education and the summary motion metric were introduced as covariates.*

Figure 10. *The ROI participation profile linked to brain-object-based movie coupling. The correlation coefficients (panel [a]) and the standardized coefficients (panel [b]) of the ROI participation variables on their corresponding canonical variate across all test CCAs, as well as the scatter plot describing the linear association between the ROI participation variate and brain-object-based movie coupling across all the "test" folds (panel [c]). The scatter plot in panel (c) is based on standardized variables. In panels (a) and (b), white boxes correspond to coefficients that were not robust across all the bootstrapping samples, as described in the text. In all these analyses, gender, handedness, years of education and the summary motion metric were introduced as covariates*. Panel (d) *Results of the Neurosynth decoding analysis constrained to the ROIs that showed robust correlations with the extracted covariate in panel (a).*

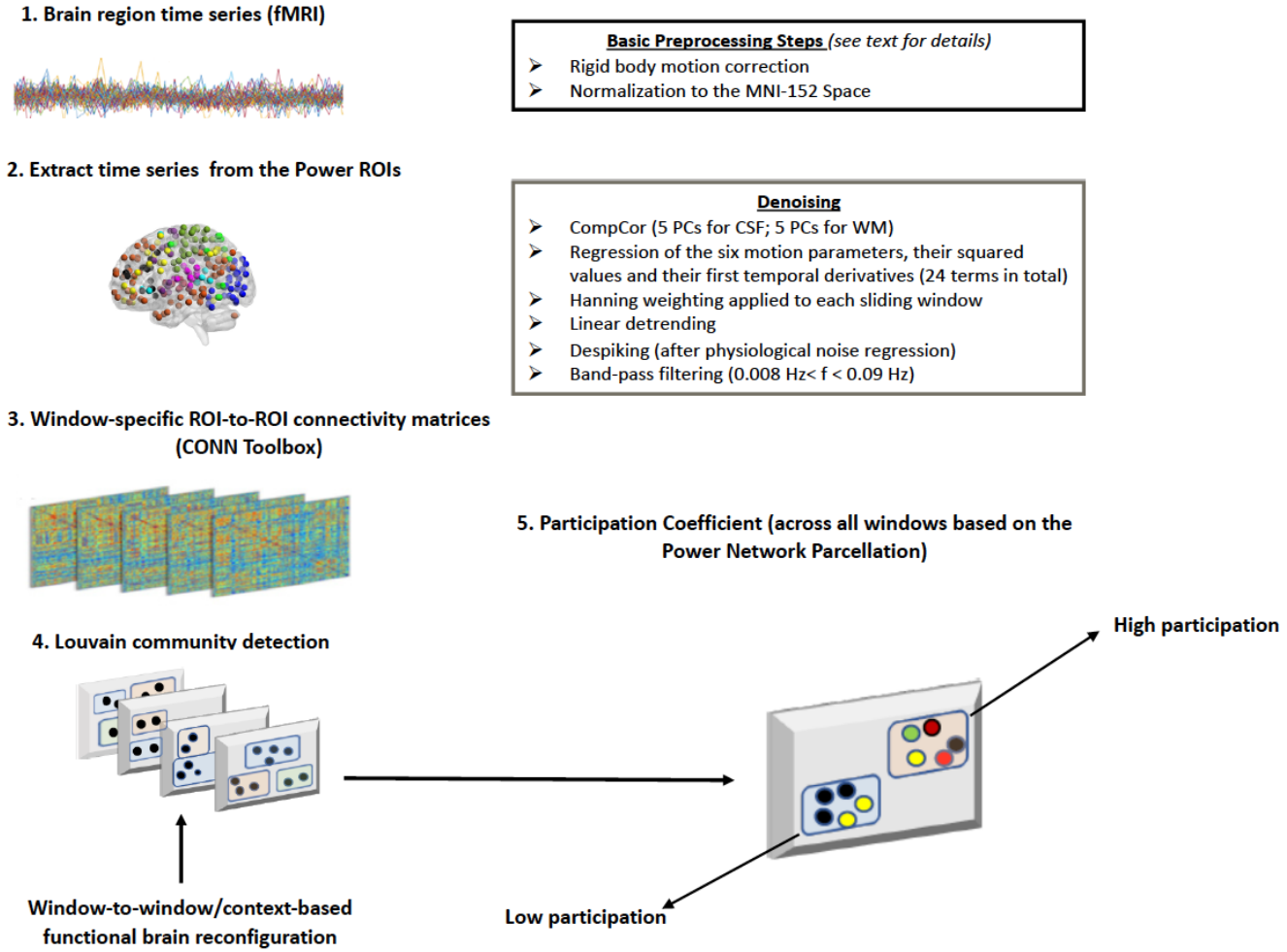

Figure 1. *Schematic representation of the main preprocessing and analysis steps across both samples.*

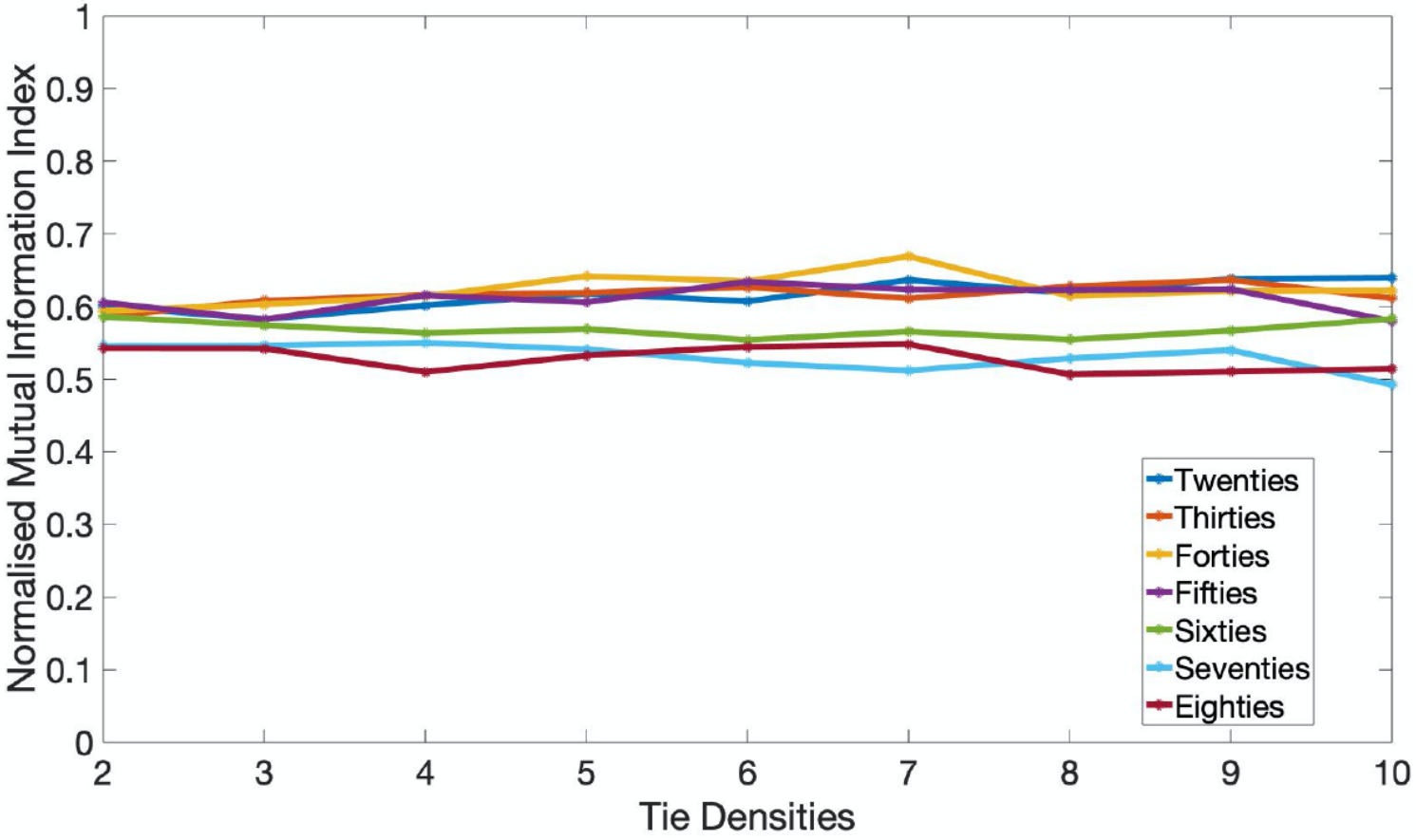

Figure 2. Network structure in each of the seven age groups of the Cam-Can sample during movie watching at 2-10% tie densities shows similar levels of similarity to that reported by Power et al.' (2011) across various cohorts during rest. The colored lines show the normalized mutual information index (NMI), a highly used metric of similarity in community assignment, for each age group and tie density scrutinized.

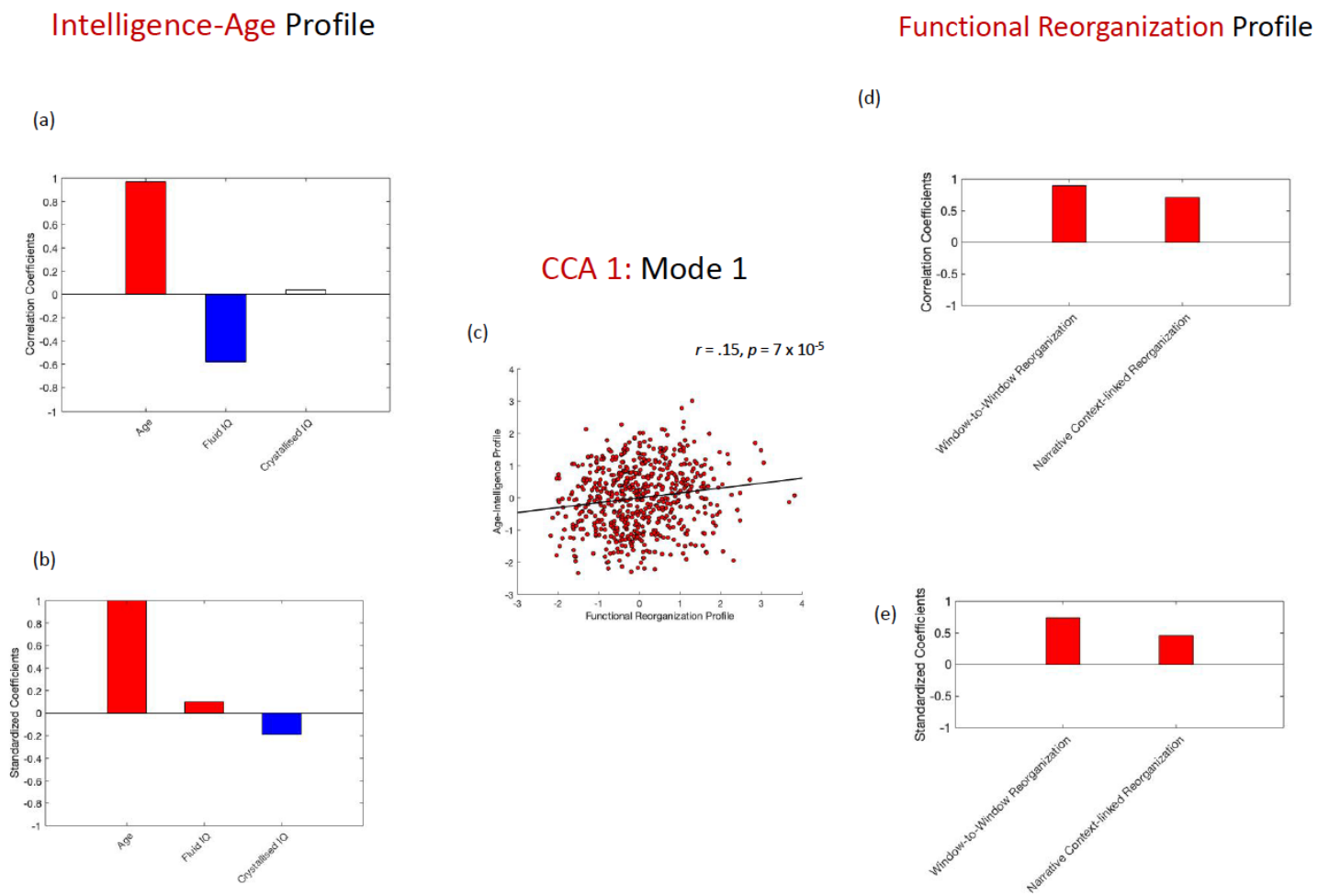

Figure 3. *Age, intelligence and functional brain reconfiguration.*

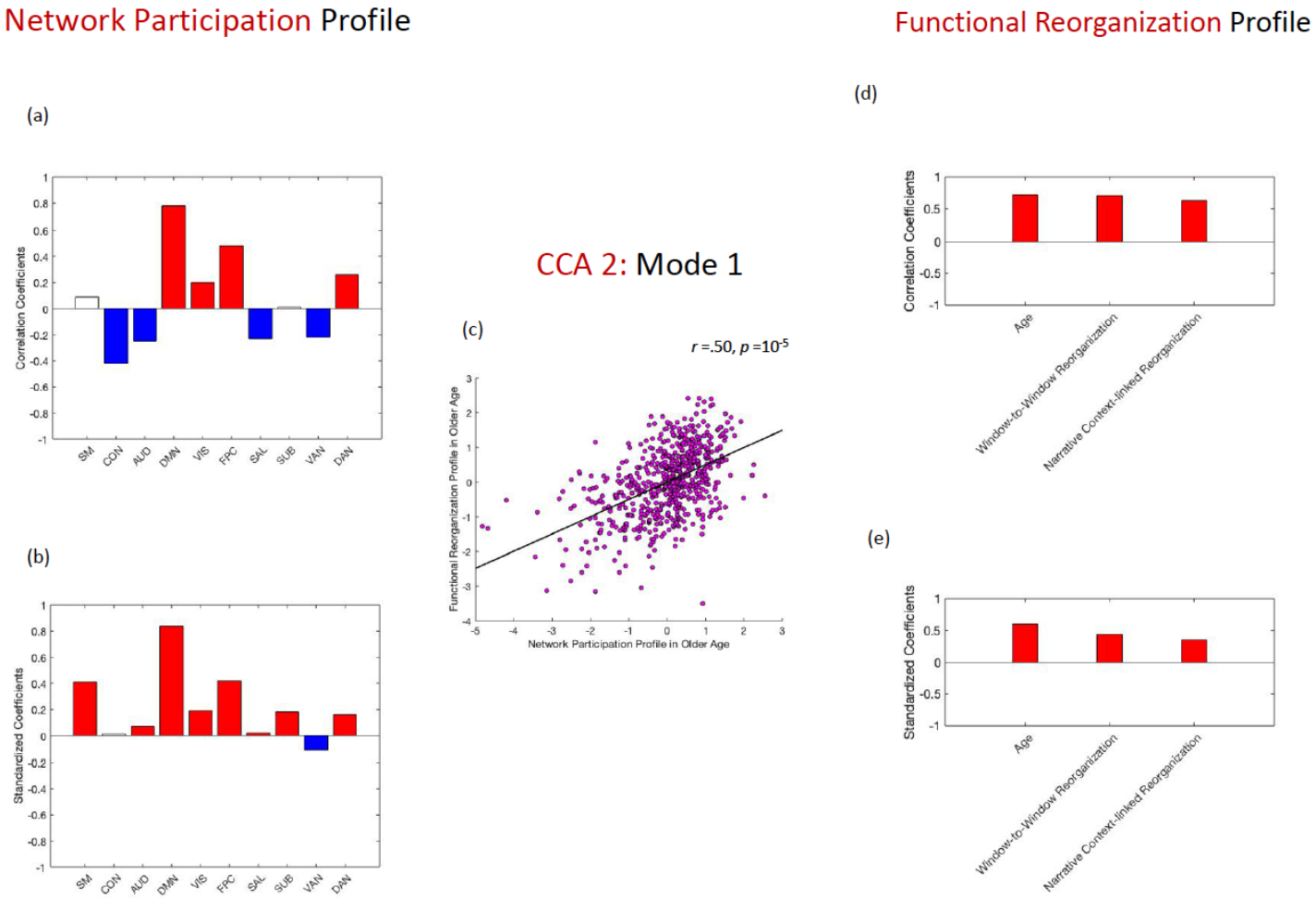

Figure 4. *Functional brain reconfiguration and network participation in older adulthood.*

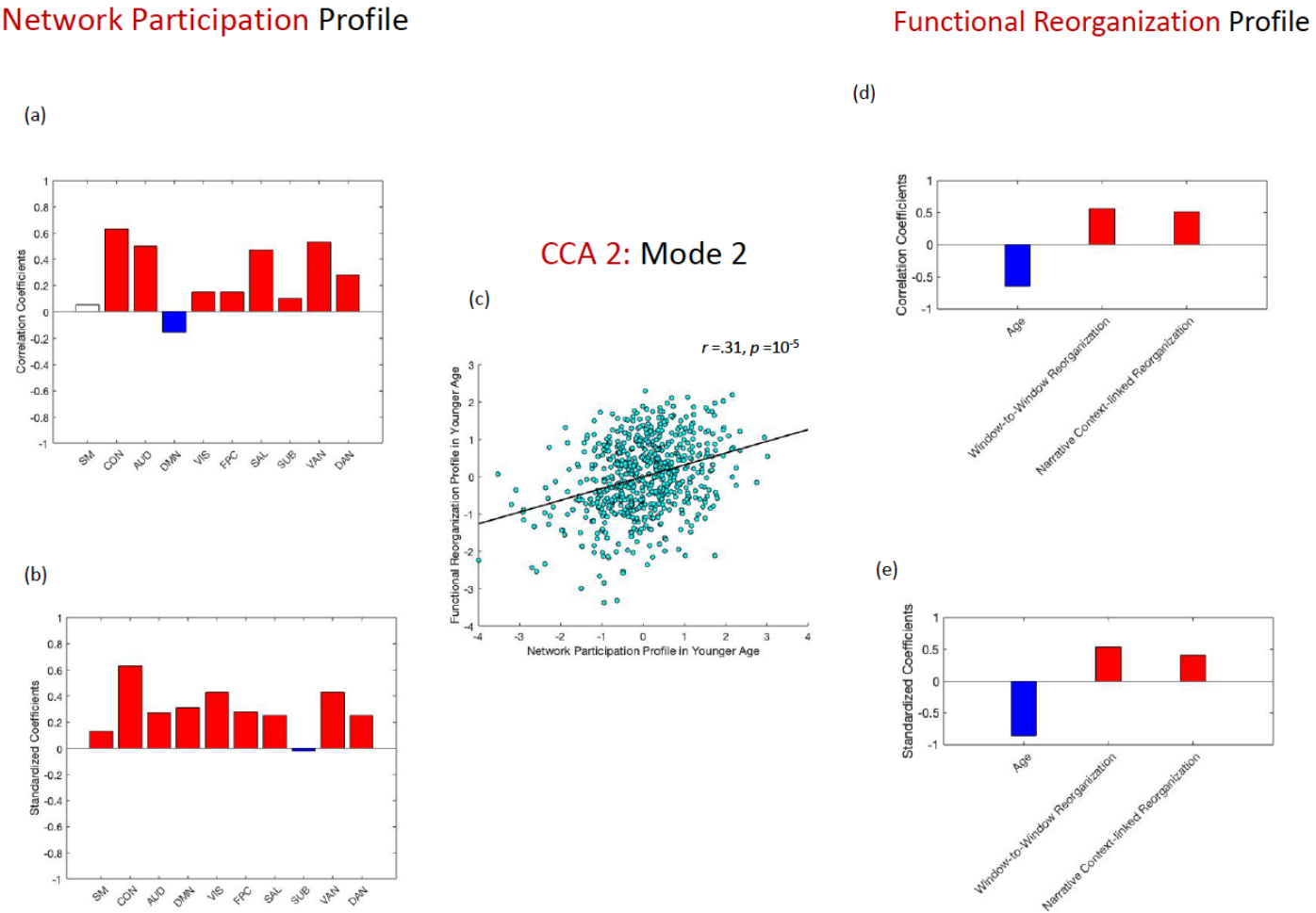

Figure 5. *Functional brain reconfiguration and network participation in younger adulthood.*

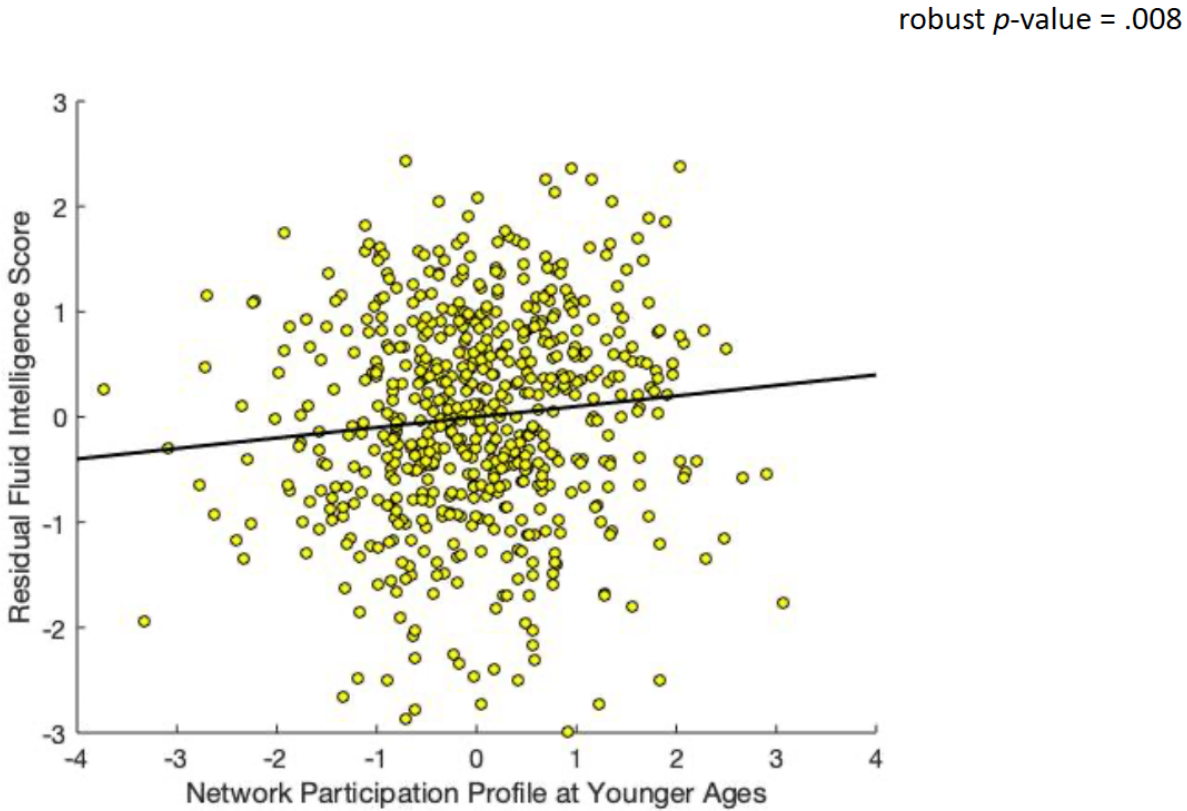

Figure 6. Scatterplot describing the association between the fluid intelligence score and the network participation profile linked to functional reconfiguration in younger adulthood, after controlling for all the covariates described in the text.

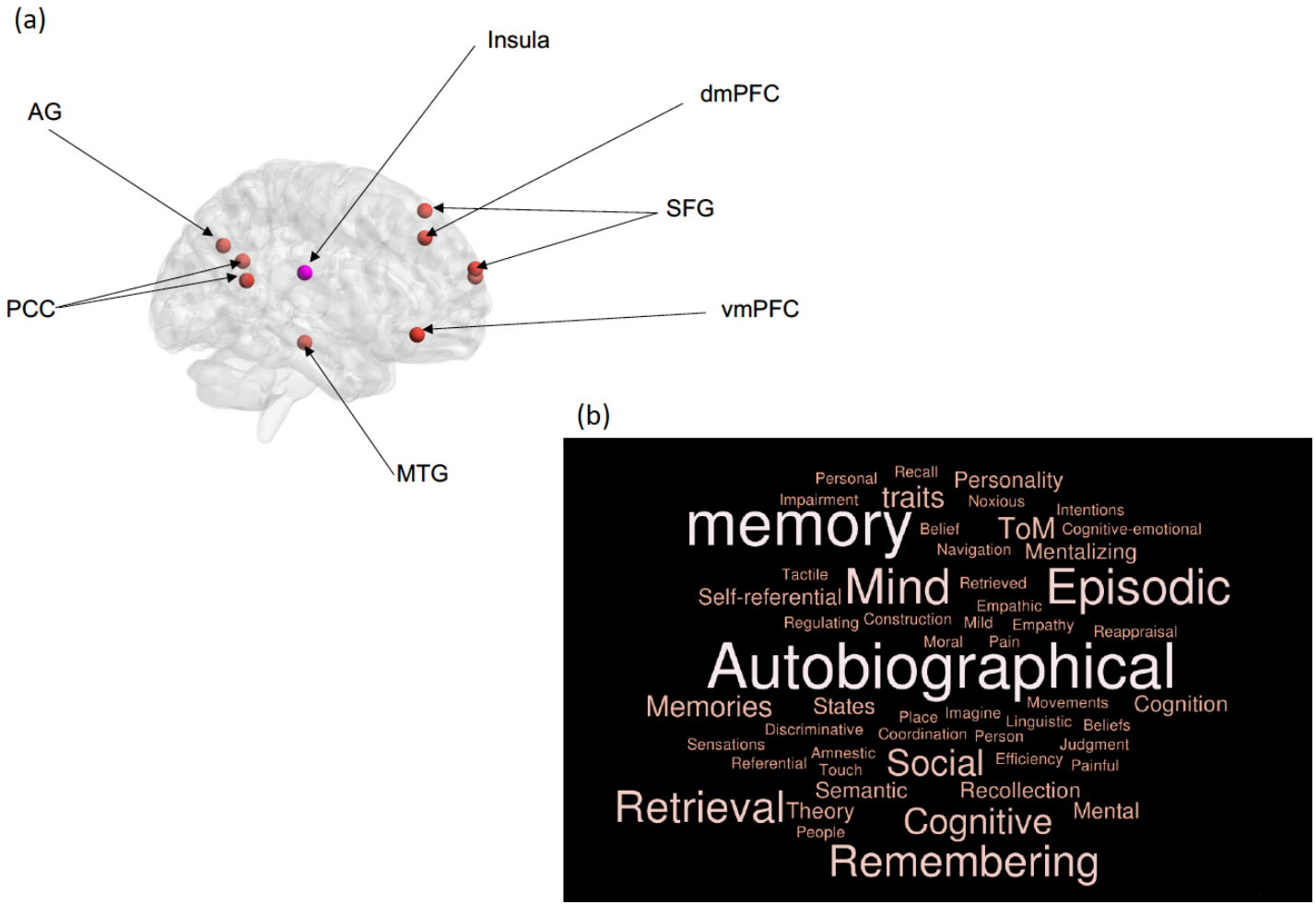

Figure 7. Panel (a). *Results of the PLS analysis, showing the ROIs that demonstrated robust associations with context-based functional brain reconfiguration across the lifespan.* Panel (b) *Results of the Neurosynth decoding analysis based on the ROIs in panel (a).*

(a)

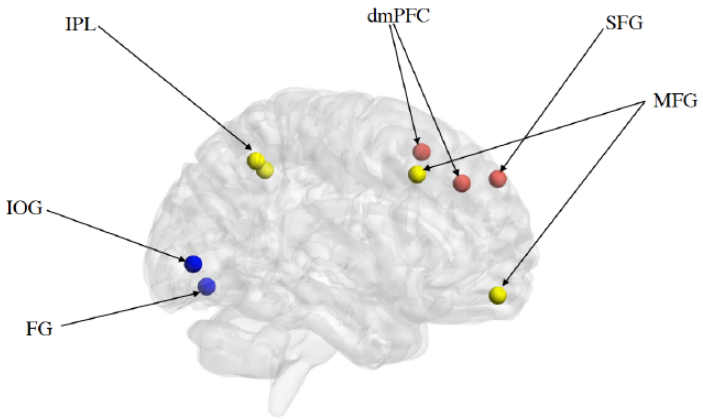

(b)

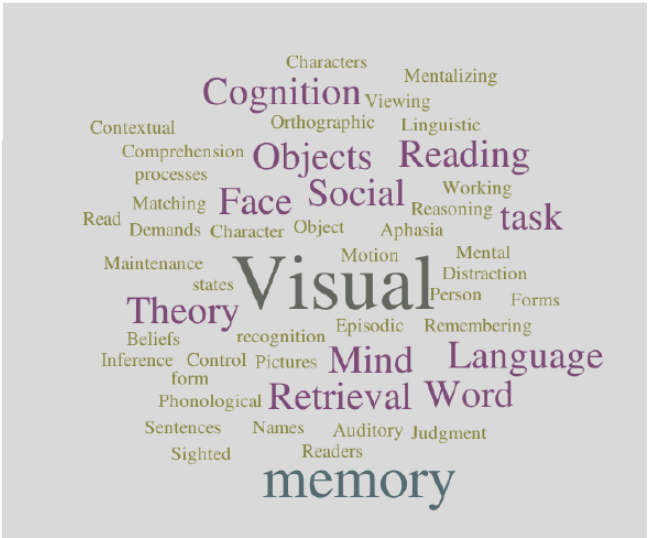

Figure 8. Panel (a). *Results of the PLS analysis, showing the ROIs that demonstrated robust associations with window-to-window functional brain reconfiguration across the lifespan.* Panel (b) *Results of the Neurosynth decoding analysis based on the ROIs in panel (a).*

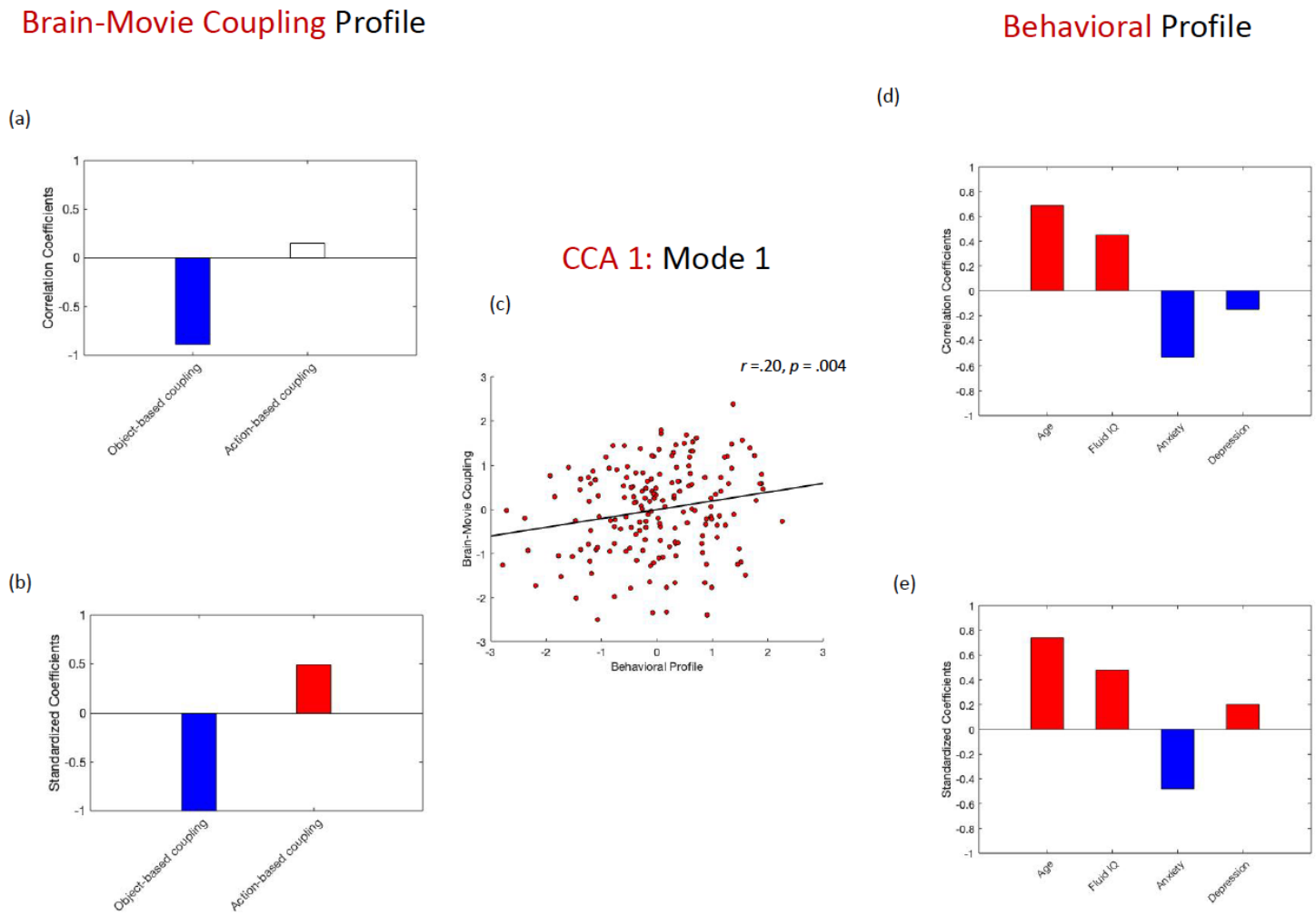

Figure 9. *Brain-movie coupling and cognitive-affective function in the HCP sample*.

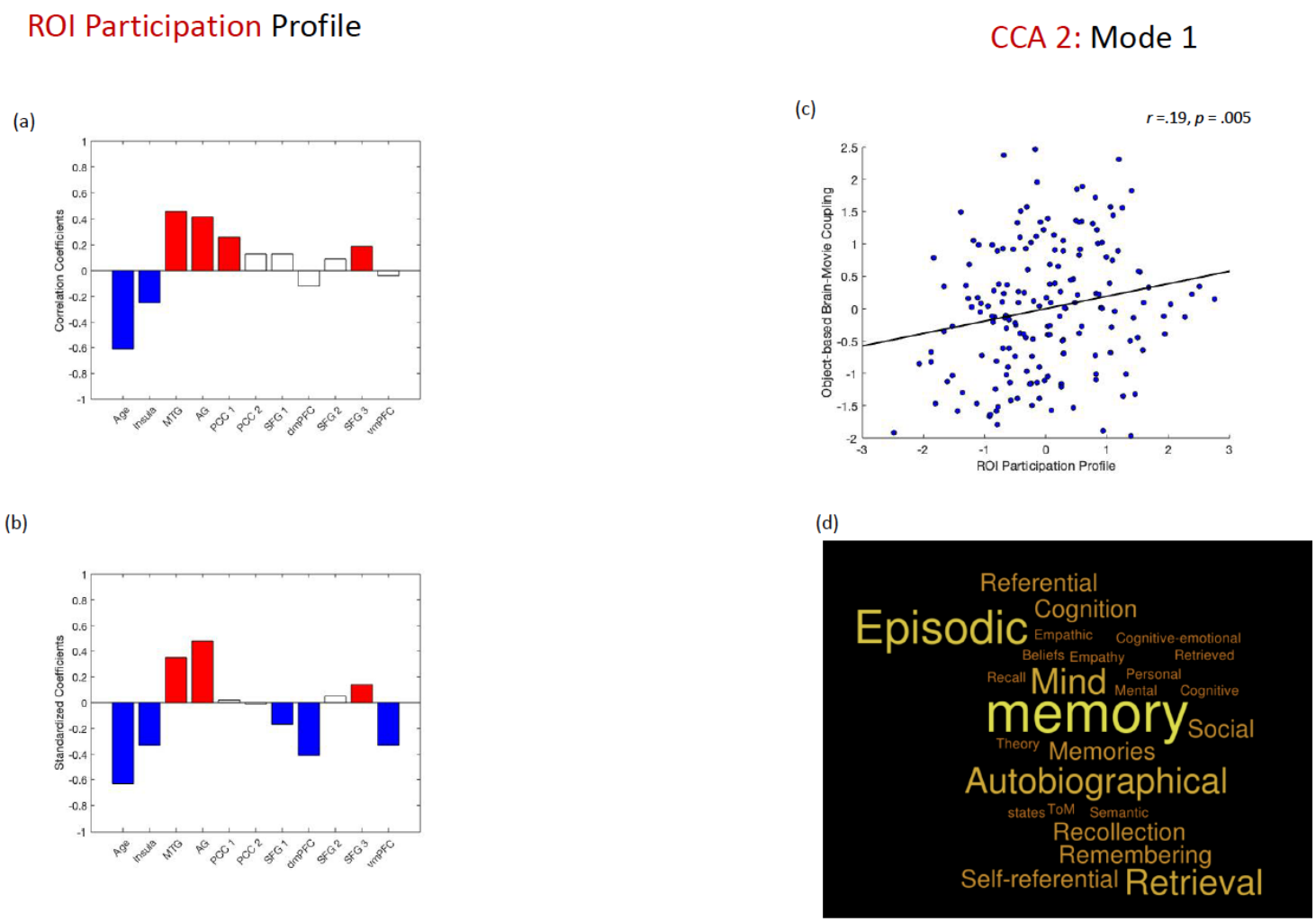

Figure 10. *The ROI participation profile linked to brain-object-based movie coupling.*